U.S. Department
of Transportation
Federal Railroad
Administration

Office of Research,
Development and Technology
Washington, DC 20590

Finite Element Analyses of Side Impacts to DOT-113 Surrogate Tank Cars with Water and Liquid Nitrogen

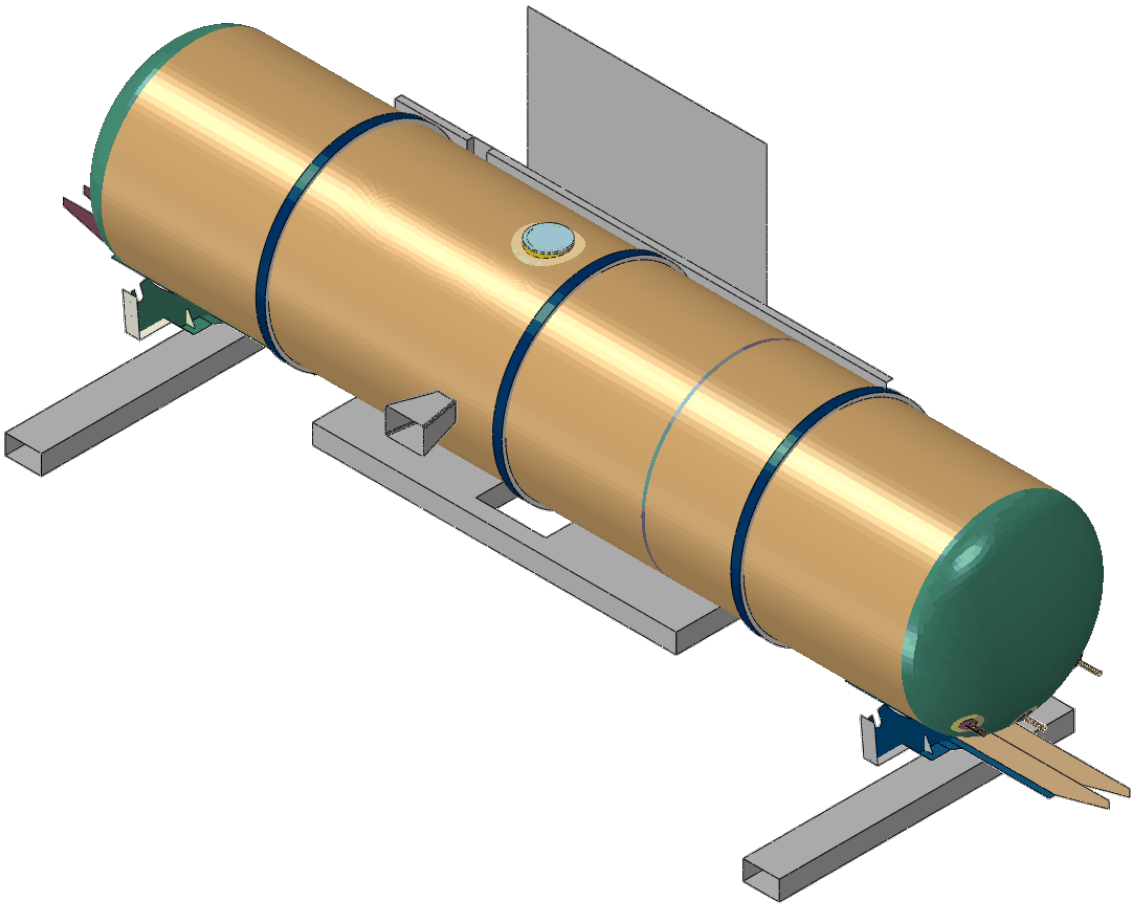

DOT/FRA/ORD-22/22

Final Report | June 2022

REPORT DOCUMENTATION PAGE

Form Approved
OMB No. 0704-0188

1. REPORT DATE *(DD-MM-YYYY)*	**2. REPORT TYPE**	**3. DATES COVERED** *(From - To)*
June 2022	Technical Report	June 11, 2020 to May 10, 2021

4. TITLE AND SUBTITLE
Finite Element Analyses of Side Impacts to DOT-113 Surrogate Tank Cars with Water and Liquid Nitrogen

5a. CONTRACT NUMBER

5b. GRANT NUMBER

5c. PROGRAM ELEMENT NUMBER

6. AUTHOR(S)
Shaun Eshraghi 0000-0002-8152-0838
Aswani Krishnamurthy 0000-0003-3116-7797
Michael Carolan 0000-0002-8758-5739

5d. PROJECT NUMBER
RR28A520

5e. TASK NUMBER
UK387

5f. WORK UNIT NUMBER

7. PERFORMING ORGANIZATION NAME(S) AND ADDRESS(ES)
Volpe National Transportation Systems Center
55 Broadway
Cambridge, MA 02142

8. PERFORMING ORGANIZATION REPORT NUMBER

9. SPONSORING/MONITORING AGENCY NAME(S) AND ADDRESS(ES)
U.S. Department of Transportation
Federal Railroad Administration
Office of Railroad Policy and Development
Office of Research, Development and Technology
Washington, DC 20590

10. SPONSOR/MONITOR'S ACRONYM(S)

11. SPONSOR/MONITOR'S REPORT NUMBER(S)
DOT/FRA/ORD-22/22

12. DISTRIBUTION/AVAILABILITY STATEMENT
This document is available to the public through the FRA website.

13. SUPPLEMENTARY NOTES
COR: Francisco González, III

14. ABSTRACT

On June 11, 2022, the Federal Railroad Administration (FRA) conducted a side impact test on a surrogate DOT-113 tank car filled with water at the Transportation Technology Center (TTC) to (1) evaluate its performance under dynamic impact conditions and (2) provide data for the verification and refinement of a computational model. The tank car was filled with water to approximately 82.4 percent of its volume, sealed, and pressurized to 50 psig. The tank car was impacted at 17.3 mph by a 297,200-pound ram car with 12-inch by 12-inch ram head fitted to the ram car. The impact caused significant deformation of the tank, but did not result in puncture of the inner or outer vessels. The Volpe National Transportation Systems Center (Volpe) performed finite element (FE) computational modeling to estimate the overall response of the tank to the impact and achieved excellent agreement with the test results.

The next side impact test took place in May 2022 with a surrogate DOT-113 tank car filled to 95 percent of its volume with liquefied nitrogen and pressurized to 50 psig. As this was the first side impact test of a tank car filled with a cryogenic liquid, Volpe conducted a series of pre-test FE modeling studies to estimate the response of the surrogate DOT-113 tank car filled with LN2. The computational studies focused on the (1) thermal contraction of the inner vessel, (2) physical behavior of cryogenic gaseous nitrogen, and (3) physical behavior of liquid nitrogen.

15. SUBJECT TERMS
Impact test, DOT-113 tank car, tank car performance, transportation safety, liquefied natural gas, LNG, liquid nitrogen, LN2, finite element analysis, FEA, hazardous materials, rolling stock, cryogenic

16. SECURITY CLASSIFICATION OF:			**17. LIMITATION OF ABSTRACT**	**18. NUMBER OF PAGES**	**19a. NAME OF RESPONSIBLE PERSON**
a. REPORT	**b. ABSTRACT**	**c. THIS PAGE**			Francisco González, III
Unclassified	Unclassified	Unclassified		63	**19b. TELEPHONE NUMBER** *(Include area code)* 202-493-6076

Standard Form 298 (Rev. 8/98)
Prescribed by ANSI Std. Z39.18

METRIC/ENGLISH CONVERSION FACTORS

ENGLISH TO METRIC

LENGTH (APPROXIMATE)

1 inch (in)	=	2.5 centimeters (cm)
1 foot (ft)	=	30 centimeters (cm)
1 yard (yd)	=	0.9 meter (m)
1 mile (mi)	=	1.6 kilometers (km)

AREA (APPROXIMATE)

1 square inch (sq in, in^2)	=	6.5 square centimeters (cm^2)
1 square foot (sq ft, ft^2)	=	0.09 square meter (m^2)
1 square yard (sq yd, yd^2)	=	0.8 square meter (m^2)
1 square mile (sq mi, mi^2)	=	2.6 square kilometers (km^2)
1 acre = 0.4 hectare (he)	=	4,000 square meters (m^2)

MASS - WEIGHT (APPROXIMATE)

1 ounce (oz)	=	28 grams (gm)
1 pound (lb)	=	0.45 kilogram (kg)
1 short ton = 2,000 pounds (lb)	=	0.9 tonne (t)

VOLUME (APPROXIMATE)

1 teaspoon (tsp)	=	5 milliliters (ml)
1 tablespoon (tbsp)	=	15 milliliters (ml)
1 fluid ounce (fl oz)	=	30 milliliters (ml)
1 cup (c)	=	0.24 liter (l)
1 pint (pt)	=	0.47 liter (l)
1 quart (qt)	=	0.96 liter (l)
1 gallon (gal)	=	3.8 liters (l)
1 cubic foot (cu ft, ft^3)	=	0.03 cubic meter (m^3)
1 cubic yard (cu yd, yd^3)	=	0.76 cubic meter (m^3)

TEMPERATURE (EXACT)

[(x-32)(5/9)] °F = y °C

METRIC TO ENGLISH

LENGTH (APPROXIMATE)

1 millimeter (mm)	=	0.04 inch (in)
1 centimeter (cm)	=	0.4 inch (in)
1 meter (m)	=	3.3 feet (ft)
1 meter (m)	=	1.1 yards (yd)
1 kilometer (km)	=	0.6 mile (mi)

AREA (APPROXIMATE)

1 square centimeter (cm^2)	=	0.16 square inch (sq in, in^2)
1 square meter (m^2)	=	1.2 square yards (sq yd, yd^2)
1 square kilometer (km^2)	=	0.4 square mile (sq mi, mi^2)
10,000 square meters (m^2)	=	1 hectare (ha) = 2.5 acres

MASS - WEIGHT (APPROXIMATE)

1 gram (gm)	=	0.036 ounce (oz)
1 kilogram (kg)	=	2.2 pounds (lb)
1 tonne (t)	=	1,000 kilograms (kg)
	=	1.1 short tons

VOLUME (APPROXIMATE)

1 milliliter (ml)	=	0.03 fluid ounce (fl oz)
1 liter (l)	=	2.1 pints (pt)
1 liter (l)	=	1.06 quarts (qt)
1 liter (l)	=	0.26 gallon (gal)
1 cubic meter (m^3)	=	36 cubic feet (cu ft, ft^3)
1 cubic meter (m^3)	=	1.3 cubic yards (cu yd, yd^3)

TEMPERATURE (EXACT)

[(9/5) y + 32] °C = x °F

QUICK INCH - CENTIMETER LENGTH CONVERSION

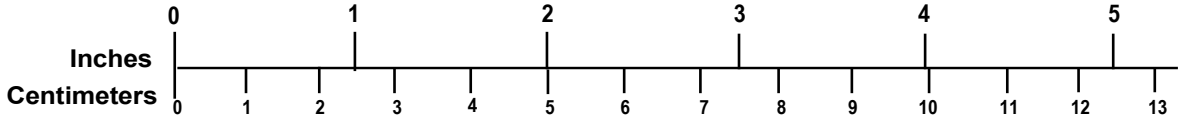

QUICK FAHRENHEIT - CELSIUS TEMPERATURE CONVERSIO

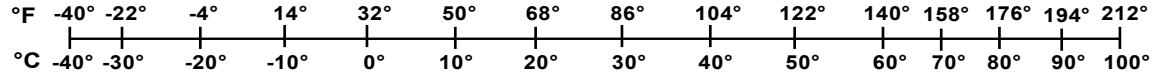

For more exact and or other conversion factors, see NIST Miscellaneous Publication 286, Units of Weights and Measures. Price $2.50 SD Catalog No. C13 10286

Updated 6/17/98

Acknowledgements

The authors of this report gratefully acknowledge the cooperation and assistance of Hector Villarreal and Devangkumar Patel of Taylor-Wharton Americas in providing engineering drawings and design information for the DOT-113 tank car surrogate used in the modeling described in this report.

Additionally, inputs from Francisco González, III of the Federal Railroad Administration's Office of Research, Development and Technology were valuable in developing the modeling described in this report and the companion testing program.

Contents

Illustrations

Tables

Executive Summary

From June 2020 to May 2021, the Federal Railroad Administration (FRA) worked with the Volpe National Transportation Systems Center (Volpe) to analyze the side impact puncture performance of a surrogate DOT-113 tank car filled with cryogenic liquid nitrogen (LN2) in anticipation of performing an impact test under this loading condition. Since this would be the first side impact test using LN2, a series of incremental analyses was performed to transition from a validated post-test model of a DOT-113 surrogate filled with water at room temperature to a pre-test model of a DOT-113 surrogate filled with LN2 at cryogenic temperature. The test of a DOT-113 surrogate filled with LN2 was the third test in a planned series of four tests on DOT-113 tank cars and surrogates.

Volpe performed pre-test analyses of the DOT-113 surrogate filled with water (Test 11), and on June 11, 2020, the impact test was conducted at the Transportation Technology Center, Inc. (TTCI) meeting all the test requirements. The surrogate tank car was impacted by a 297,200-pound ram car fitted with a 12-inch by 12-inch ram head traveling at 17.3 mph. The impact resulted in a significant amount of deformation but did not puncture the tank car. After the test, Volpe updated the pre-test finite element (FE) model to represent the measured speed of the ram car resulting in excellent agreement with the measured test data. FRA documents the results of this testing and modeling effort in a separate report [2].

While Volpe's analysis of Test 11 compared well with the test results, the next test in the series (Test 12) presented several technical challenges to conducting pre-test analyses. This report documents the technical challenges and modeling approach in transitioning from analyzing a DOT-113 surrogate filled with water to one filled with LN2.

The post-test model from Test 11 was incrementally simplified to represent a generalized DOT-113 surrogate with the initial conditions from Test 11. The generalized model was still in good agreement with the test results even though it did not feature many details of the surrogate's design. The generalized model was then incrementally modified to represent the planned test conditions for Test 12 and then documented the overall effect of each incremental change. Once the design of the Test 12 DOT-113 surrogate was finalized by the manufacturer and FRA, the generalized model was updated to represent the actual design of the DOT-113 surrogate including the actual tank dimensions, piping, stub sills, bolsters, inner vessel support, manway, etc.

Even though the geometry and materials of construction of the DOT-113 surrogate were carefully modeled, several modeling uncertainties remained including:

1. Changes to the compressibility of the gaseous nitrogen (N2) due to:
    a. Real gas intermolecular interactions
    b. Phase change
    c. Non-uniform temperature distribution
    d. Convective heat transfer

2. Changes to the plasticity and fracture of the inner vessel's stainless steel due to:
    a. Cryogenic temperature
    b. Elevated strain rate
    c. Heat generation

After the model uncertainties were investigated, a parametric study of the puncture speed range determined the impact speed for Test 12. FRA's report describes the puncture model results for Test 12 [2].

1. Introduction

This report documents pre-test analyses for a side impact test performed on a surrogate DOT-113 tank car filled with liquefied nitrogen (LN2). A DOT-113 is a specially-designed tank car intended to transport cryogenic liquid commodities. Previous tank car tests in the Federal Railroad Administration's (FRA) side impact testing program have used water as a stand-in for the intended service lading, e.g., chlorine, crude oil, liquefied natural gas (LNG), etc. As this test was the first test using a cryogenic liquid lading, a series of analyses were performed to incrementally examine the effects that a cryogenic liquid would have on the mechanical behavior of the gas and fluid inside the tank and the inner vessel's material properties.

1.1 Background

In the past decade, significant research has been conducted to analyze and improve the impact behavior and puncture resistance of railroad tank cars. Ultimately, the results of this research will be used by Federal regulatory agencies—i.e., FRA and the Pipeline and Hazardous Materials Safety Administration (PHMSA) in the United States—to establish performance-based testing requirements and to develop methods to evaluate the crashworthiness and structural integrity of different tank car designs when subjected to a standardized shell impact scenario. A performance-based requirement for tank car head impact protection has already been defined within the current regulations [3], and an optional performance-based requirement for tank car shell impact resistance is applicable to DOT-117P tank cars [4].

FRA has a continuing research program to provide the technical basis for rulemaking on enhanced and alternative performance standards for tank cars and review of new and innovative designs that are developed by the industry and other countries. In support of this ongoing research program, full-scale tests are necessary to provide the technical information to validate modeling efforts and to inform regulatory activities. These tests evaluate the crashworthiness performance of tank cars used in the transportation of hazardous materials including designs that comply with current regulations as well as innovative new designs that have improved puncture resistance.

A DOT-113 tank car is a specialized tank car that is designed to transport cryogenic liquids.[1] A cryogenic liquid is "a refrigerated liquefied gas having a boiling point colder than -90 °C (-130 °F) at 101.3 kPa (14.7 psia) absolute."[2] DOT-113 tank cars are "tank-within-a-tank" cars, where the inner vessel is in contact with the cryogenic material and resists the pressure exerted by the lading, and an outer vessel surrounds the inner vessel and insulating materials and carries the in-train forces. The DOT-113 tank car surrogate used in this test was constructed specifically for use in this shell impact test. The surrogate included design features representative of a specification DOT-113 tank car, including typical materials of construction for the inner and outer vessels, typical diameters for the inner and outer vessel shells, typical thicknesses for the inner and outer vessels, and typical pressure relief valve (PRV) arrangements. The surrogate did

[1] Pipeline and Hazardous Materials Safety Administration, DOT, Title 49 Code of Federal Regulations (CFR) § 179.302 Subpart F–Specification for Cryogenic Liquid Tank Car Tanks and Seamless Steel Tanks (Classes DOT-113 and 107A), Retrieved from U.S. Government Publishing Office.

[2] 49 CFR § 173.115(g)–Class 2, Divisions 2.1, 2.2, and 2.3 - Definitions, *Cryogenic liquid*.

not include features required of tank cars that would not have an effect on the puncture response during a shell impact, such as couplers, trucks, brake piping, or safety appliances. The terms "surrogate" and "tank car surrogate" are used interchangeably throughout this report.

The Hazardous Materials Regulations (HMR) permits the transportation of several cryogenic liquids via DOT-113 tank cars, including argon and ethylene. Methane, refrigerated liquid (more commonly referred to as LNG) was not authorized for transportation via DOT-113 tank car prior to 2020. On October 2019, PHMSA and FRA published a Notice of Proposed Rulemaking (NPRM) [3] that would permit LNG to be transported in DOT-113 tank cars. Because the existing fleet of DOT-113 tank cars is small compared to the overall tank car fleet and limited accident data exists regarding the performance of these cars in derailments or collisions, a series of full-scale shell impact tests was planned to provide technical information on the puncture resistance of the DOT-113 tank car. In November 2019, the first test in this series was performed [1]. In June 2020, the second test in this series was performed [2].

DOT-113 tank cars include several unique design features that are not found on non-pressure (e.g., DOT-117) or pressure (e.g., DOT-105) tank cars because of the particular properties of cryogenic materials. The inner vessel of a DOT-113 tank car will be exposed to cryogenic temperatures and must be constructed of either ASTM A240 Type 304 or Type 304L stainless steel [5]. Those grades of steel maintain desirable properties at cryogenic temperatures. Since the inner vessel and lading must be kept at cryogenic temperatures during transit, the inner vessel must be surrounded by highly-effective insulation. This insulation may take the form of expanded perlite (i.e., a granular lightweight natural mineral) or multiple layers of "super" insulating materials (i.e., multi-layer insulation [MLI]). Additionally, a vacuum is typically used in conjunction with either perlite or multi-layer insulation to further reduce heat transfer into the inner vessel. The specification defines a maximum rate of heat transfer that is permissible through the insulation system. The inner vessel and insulation must be surrounded by an external tank to contain the insulation, maintain the vacuum, and carry the in-train forces.

1.2 Objectives

The overall objective of the modeling program is to develop finite element (FE) models capable of estimating the impact response and puncture behavior of the outer and inner vessels of a DOT-113 tank car under cryogenic conditions. The objective of the modeling described in this report was to document the relative effects of several behaviors known to differ between water at ambient temperature and LN2 at cryogenic temperatures on the impact response of a DOT-113 tank car surrogate.

1.3 Overall Approach

FRA conducted side impact tests on DOT-105, DOT-111, DOT-112, DOT-117, and DOT-113 tank cars. These tests were all accompanied by companion FE analysis. These tests covered a wide range of tank car designs (e.g., capacities, shell diameter, shell thickness, vintage, manufacturer, outage level, outage pressure, etc.) The ultimate goal of the tank car shell impact testing and modeling program is to understand how a particular tank car performs under a

[3] Regulations.gov, Federal Register/Vol 84, No. 206–Hazardous Materials: Liquefied Natural Gas by Rail, October 24, 2019.

standardized impact scenario that is representative of typical service conditions. For a DOT-113 tank car, typical service conditions mean a cryogenic commodity within the inner vessel. The overall approach to understanding the behaviors of a DOT-113 tank car under impact conditions and the potential for improvement to its performance through design changes uses full-scale and laboratory testing with companion FE modeling of increasing complexity to ultimately represent a DOT-113 tank car under LNG service conditions subjected to a shell impact that punctures both inner and outer vessels. The planned approach includes future tests and corresponding analyses to examine the influence of different materials/thicknesses used for the tank shell, examine the effect(s) of modeling both the lading and the inner vessel steel using properties at cryogenic conditions, and ultimately modeling a DOT-113 tank car under "representative" conditions expected for LNG service as shown in Table 1.

Table 1. Planned DOT-113 Side Impact Test Series

Test #	Date	Test Article	Lading	Report
10	November 2019	Legacy DOT-113	Water	[1]
11	June 2020	Surrogate DOT-113	Water	[2]
12	July 2021	Surrogate DOT-113	LN2	TBD
13	TBD	New DOT-113	LN2	TBD

Observations, lessons learned, and data collected during the first two impact tests of a DOT-113 tank car and tank car surrogate were used as a starting point for the technically challenging task of modeling of the DOT-113 surrogate filled with LN2. The major difference between this third test and the previous two tests in this series is the use of LN2 in this test. A further complexity for designs such as the DOT-113 is the consideration of puncture of one or both tanks.

Volpe and FRA collaborated with the Pipeline and Hazardous Materials Safety Administration (PHMSA) to determine the targeted outage, pressure, and temperature of the DOT-113 surrogate filled with LN2. After determining the targeted initial conditions, Volpe conducted extensive pre-test modeling to quantify the level of uncertainty in the speed to cause puncture of the DOT-113 surrogate. The pre-test model results are used in discussions with Volpe, FRA, and TTCI to determine a targeted impact speed for each test.

1.4 Scope

This report includes a discussion of developing and executing the FE models used in this program. Aspects of developing and executing the FE models include modeling the tank car steels, modeling water and LN2 within the tank, and modeling room temperature and cryogenic gas within the tank.

This report does not compare the analyses with the test results as that comparison will be made in the test report on the side impact test of the DOT-113 surrogate filled with LN2. This report also does not examine the puncture behavior(s) of either the outer tank's TC-128B carbon steel or the inner vessel's T304 stainless steel.

1.5 Organization of the Report

This report is structured as the following:

Section 1 introduces the work and offers an overview.

Section 2 describes the modeling thermal contraction of the DOT-113 surrogate's inner vessel.

Section 3 depicts the technical challenges of modeling a gas while considering intermolecular forces, the volume occupied by the gas's molecules, and condensation of the gas to a liquid.

Section 4 describes the properties of LN2 and modeling its sensitivity to temperature.

Section 5 includes a summary of the report and contains concluding remarks.

Appendix A describes the non-puncture FE model of the DOT-113 surrogate filled with LN2 presented in this report.

Appendix B describes the simplified model of thermal contraction of the inner vessel considering through-thickness effects.

2. Thermal Contraction of Inner Vessel

The inner vessel of the DOT-113 surrogate tank cars used in Test 11 and planned for Test 12 were both constructed from ASTM A240 Type 304 stainless steel (T304). The DOT-113 surrogate for Test 12 was expected to be transported in an empty state to the TTC and positioned against the impact wall. The test plan then called for the inner vessel to be chilled with cold gaseous nitrogen to reduce the temperature of the inner vessel so that it could be safely filled with LN2.

This section describes the modeling of the inner vessel's thermal contraction in two stages. The first stage used a simplified representation of only the inner vessel with solid elements to determine how long it would take to reach a uniform steady state temperature profile across the 0.25-inch thickness of the inner vessel. The second stage used a detailed shell element model of the entire DOT-113 surrogate to characterize the initial stress state due to thermal contraction, pressurization of the inner vessel, depressurization of the annular space, and gravity.

The results of the analyses indicated that steady-state would be reached quickly and that the initial stress due to gravity and thermal contraction could be excluded from the side impact analyses.

2.1 Thermal Contraction of Simplified DOT-113 Surrogate

The objective of this effort was to identify the need for including thermal conductivity and specific heat properties of stainless steel in the analysis process to achieve the steady state condition of a DOT-113 tank car's inner vessel filled with cryogenic liquid prior to simulating an impact. By including these effects, the runtime and complexity of an impact model will increase, but neglecting these effects required some justification. When lowering of the temperature of the inner vessel from ambient temperature to cryogenic temperature (i.e., in the case of LN2 at 14.7 psia, 77 K) it reduces the dimensions of the inner vessel and consequently results in pre-stressed condition at its connection points to the outer vessel. This pre-stressed steady state condition should be included in the FE model as the first step of analysis prior to subjecting the tank car to be impacted by a ram car.

To get to the cryogenic LN2 temperature of 77 K, the inner vessel was initially at ambient temperature through its thickness. While getting filled with LN2 the inner surface of the inner vessel will decrease in temperature to 77 K while the outer surface of the inner vessel will remain at ambient temperature initially. To simulate reaching a steady state condition of the inner vessel, FE analysis used the inner vessel material (T304) properties including thermal conductivity and specific heat over a range of temperatures between ambient temperature and 77 K to arrive at the steady state condition. Due to the large size of the tank car FE model, this step might result in analyses taking a long time to run, adding to the project's analysis time due to the numerous iterations to be performed.

A simpler approach would be to apply the cryogenic temperature to the whole tank car's inner vessel instantaneously. This could be assumed to be acceptable because of the diameter (d) to thickness (t) ratio of the tank car meeting the thin-walled cylinder definition ($d/t > 20$) because of the thickness being 0.25-inches compared to the ~100-inch diameter of the tank car. While in reality, the actual time taken for reaching the steady state condition through the inner vessel's

wall may not be zero, it should be small enough such that it could be assumed to reach the steady state condition quickly.

The assumption that the inner vessel reaches steady-state conditions in a short period of time requires investigation before incorporating this within the puncture-capable FE model. Thus, this analysis was performed to estimate the minimum time required for the tank car to reach the steady state when the tank car is filled with LN2 at cryogenic temperature of 77 K. To simulate this operating condition, the inner surface of the tank car was given a boundary condition of 77 K and the outer surface was given an initial temperature condition of 293 K. The model was allowed to run for sufficient time for the outer surface of the inner vessel to reach approximately 77 K over its entire surface. The effect of convection from the outer surface of the inner vessel was assumed to be negligible and hence ignored due to the large volume of LN2 that fills the inner vessel and the insulation and vacuum in between the inner and outer vessels.

The inner vessel is made of T304, and the material properties in this model used U.S. customary units (inch-lbf-second-Fahrenheit).[4] A temperature of 293 K corresponds to 68 °F and 77 K corresponds to -321 °F. Three solid elements were used to represent the 0.25-inch thickness of the tank car and four nodes represent the said thickness. Table 2 through Table 4 show the temperature dependent material properties of T304 stainless steel material including thermal expansion, thermal conductivity and specific heat respectively, which were used in performing this analysis.

Table 2. Coefficient of Thermal Expansion vs. Temperature for T304 Stainless Steel [6]

Temperature	Coefficient of Thermal Expansion
°F	*(in/in)/°F*
-452	5.709E-06
-387	6.541E-06
-342	7.006E-06
-306	7.317E-06
-270	7.581E-06
-234	7.800E-06
-198	7.980E-06
-162	8.126E-06
-126	8.241E-06
-90	8.331E-06
-54	8.399E-06
-18	8.449E-06
18	8.484E-06
54	8.481E-06
72	8.756E-06

[4] Note that the FE models presented in other sections of this report used inch-lbf-second-Kelvin

Table 3. Thermal Conductivity vs. Temperature for T304 Stainless Steel [7]

Temperature	Thermal Conductivity
°F	*lbf/s-°F*
-454	6.250E-02
-418	4.122E-01
-382	6.994E-01
-346	9.492E-01
-310	1.137E+00
-274	1.287E+00
-238	1.399E+00
-202	1.486E+00
-166	1.549E+00
-130	1.611E+00
-94	1.674E+00
-58	1.736E+00
-22	1.811E+00
14	1.874E+00
50	1.936E+00
86	2.011E+00

Table 4. Specific Heat vs. Temperature for T304 Stainless Steel [7]

Temperature	Specific Heat
°F	*in-lbf/(lbf-s^2/in-°F)*
-418	1.7222E+04
-382	5.6833E+04
-346	1.1194E+05
-310	1.6533E+05
-274	2.1097E+05
-238	2.5144E+05
-202	2.8847E+05
-166	3.1689E+05
-130	3.4186E+05
-94	3.5736E+05
-58	3.7113E+05
-22	3.8233E+05
14	3.9438E+05
50	4.0213E+05
86	4.1075E+05

Figure 1 shows the FE model of the surrogate inner vessel of the DOT-113 tank car that was used to perform this analysis. Three thermally-coupled, fully-integrated brick elements (C3D8T) were created through the thickness of the inner vessel to consider variations in temperature through the thickness. The elements measured approximately 6.7 inches in the hoop direction, 10 inches in the longitudinal direction, and 0.083 inches in thickness.

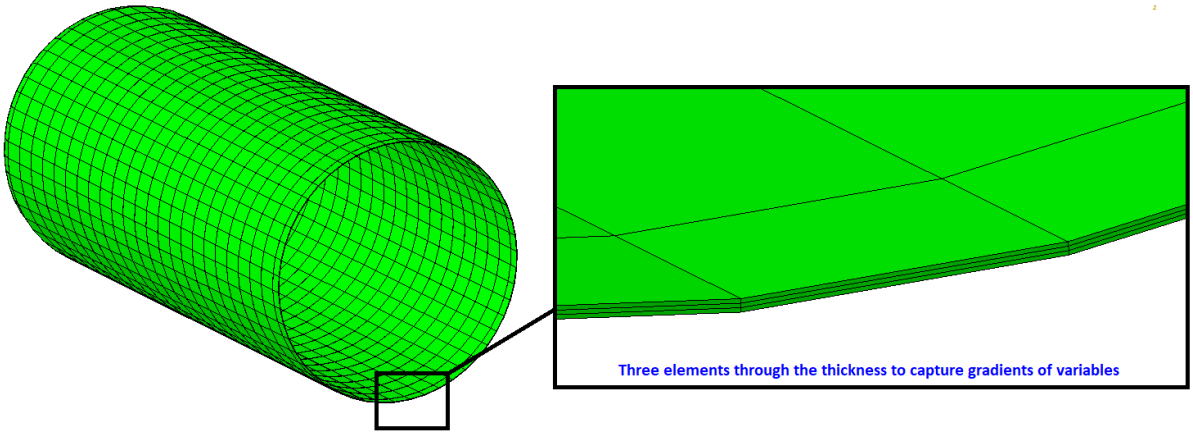

Figure 1. Sectional View of FE Model with Solid Elements Through Thickness

Figure 2 shows the temperature versus time graph for four nodes through the thickness. It can be seen that the node representing the inner surface was at 68 °F at time 0 and linearly fell to -321 °F at 15 seconds because the inner surface was given a 15 second ramping down period to prevent instability in the analysis process. The other nodes start from ambient temperature and then gradually fell reaching a steady-state condition. It is self-explanatory which nodes are located closer to the inner and outer surfaces and which nodes represent the inner and outer surfaces.

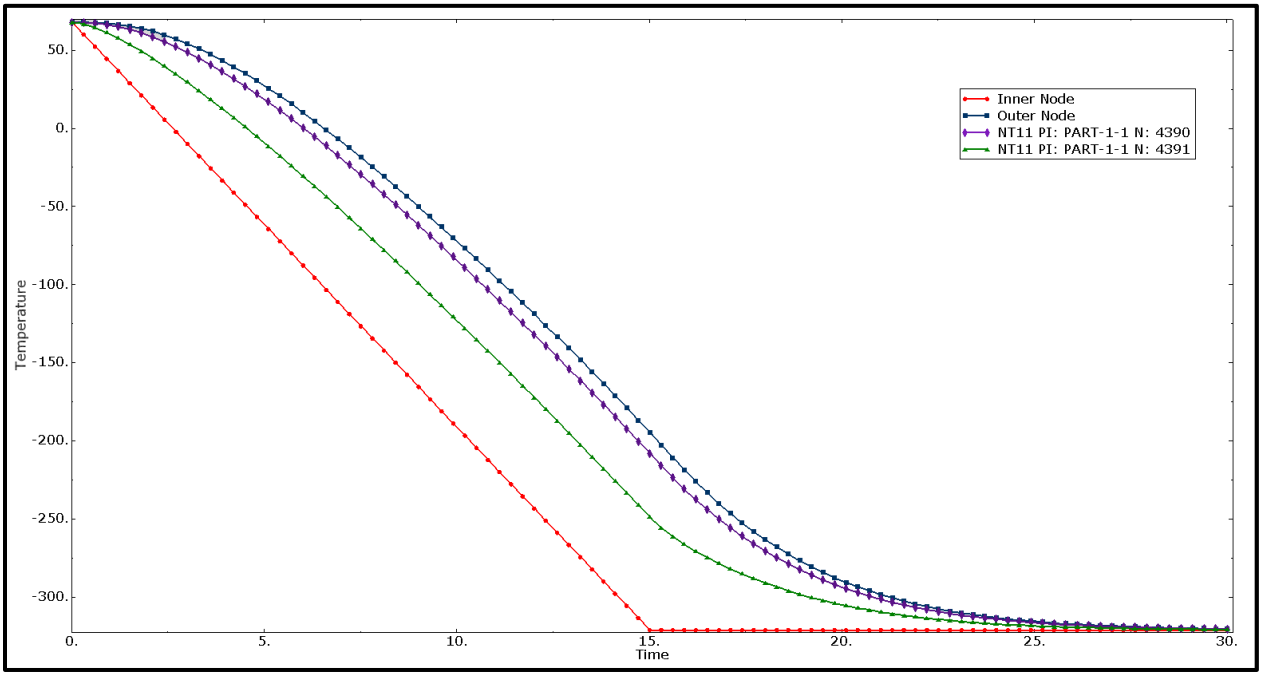

Figure 2. Temperature vs. Time for Nodes Through the Thickness

The initial inner vessel volume from the finite element analysis (FEA) model was 19,263 gallons at 68 °F. The contracted volume was 19,113 gallons at -321 °F excluding the effect of pressurization inside the inner vessel.

Based on the analysis performed, it was found that it took approximately 20 seconds for the entire inner vessel to reach a steady state of -321 °F. On the other hand, it should take longer than 20 seconds to fill a tank car with LN2 to avoid thermal shock. It can be concluded that applying temperature boundary conditions for the entire thickness of the inner vessel with representative thermal expansion properties could capture the thermally-induced stress state of the inner vessel with reasonable accuracy.

Section 2.2 describes follow-on analysis using a detailed shell element model of the full DOT-113 surrogate where the through thickness temperature effects were neglected based on the results of the modeling in this section. The detailed shell element model was used to investigate the combined effects of inner vessel thermal contraction and pressurization, annular space vacuum, and gravity.

2.2 Initial Stress State Analysis of Detailed DOT-113 Surrogate Model

After it was determined that a uniform steady-state temperature was reached across the thickness of the inner vessel in a short amount of time, a detailed non-puncture model of the DOT-113 surrogate was used to investigate the state of the DOT-113 surrogate immediately prior to impact. The model was run for 45 seconds in an explicit fully coupled thermal-stress analysis at a target time increment of $1x10^{-6}$ seconds. The model was initially at a uniform temperature of 294 K. Using a 10 second smooth step amplitude curve slowly subjected the model to:

1. Gravity
2. Thermal cooling on the inner vessel from 294 K to 77 K
3. External pressure due to atmosphere at 12.3 psia on the outer vessel
4. Internal pressure to the target test pressure of 62.3 psia on the inner vessel

This combination of external pressure and internal pressure represents the vacuum in the annular space, external pressure due to atmosphere, and targeted internal pressure of the inner vessel. The 10 second amplitude curve is shown in Figure 3.

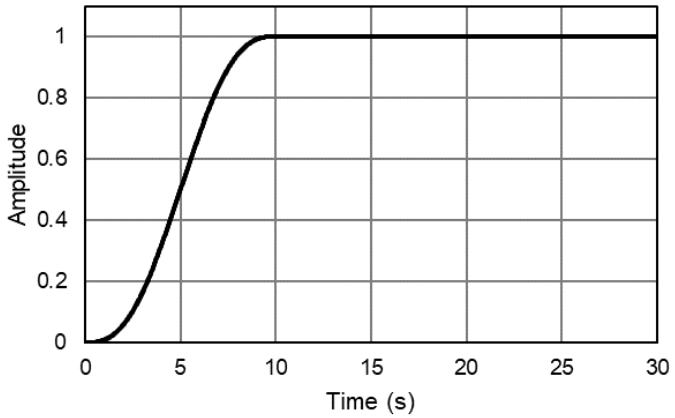

Figure 3. Smooth Step Amplitude Curve (10 seconds)

Figure 4 shows the non-puncture DOT-113 surrogate model used for the coupled thermal-stress analysis. The non-puncture/coupled thermal-stress model is similar to the non-puncture structural model described in Appendix A except it does not include (1) solid elements used to model fluid motion, (2) membrane elements used to represent the boundary of the outage, or (3) a pneumatic cavity used to represent pressurization of an ideal gas. Omitting the fluid's solid elements greatly reduced the size of the model. A non-structural mass (~104 kips) corresponding to the mass of LN2 was uniformly assigned to the inner vessel nodes up to the desired fill level ~10 inches below the top of the inner vessel (95% full). A displacement boundary condition was assigned to the rigid skids to fix their translational motion in all degrees of freedom (DOF) and their rotation parallel to the longitudinal axis of the DOT-113 surrogate tanks.

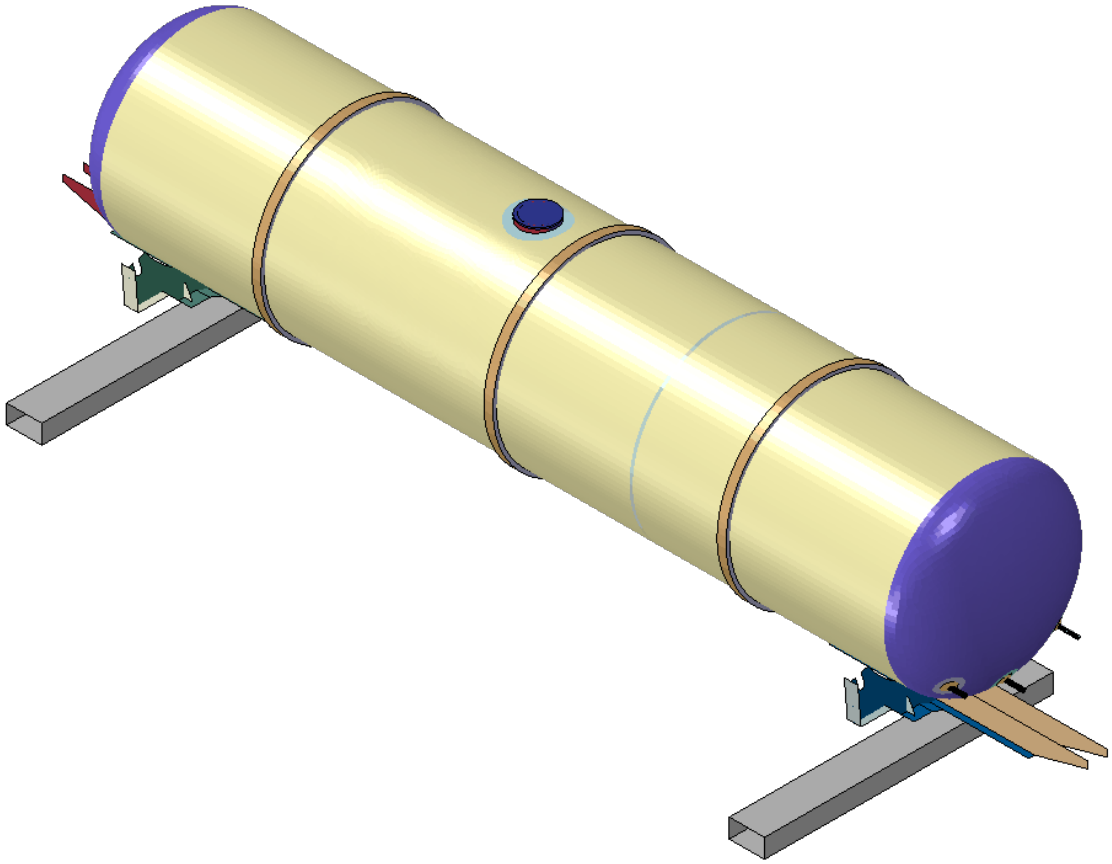

Figure 4. Non-puncture DOT-113 Surrogate FE Model Used for Coupled Thermal-stress Analysis

Figure 5 shows the vertical reaction forces at the east and west skids. The reaction force correctly accounts for the structural mass of the DOT-113 surrogate and non-structural mass of LN2. The east skid had a reaction force of 82.0 kips while the west skid had a reaction force of 83.2 kips. The slight misbalance of 1.2 kips is likely due to asymmetry in the piping and internal structures.

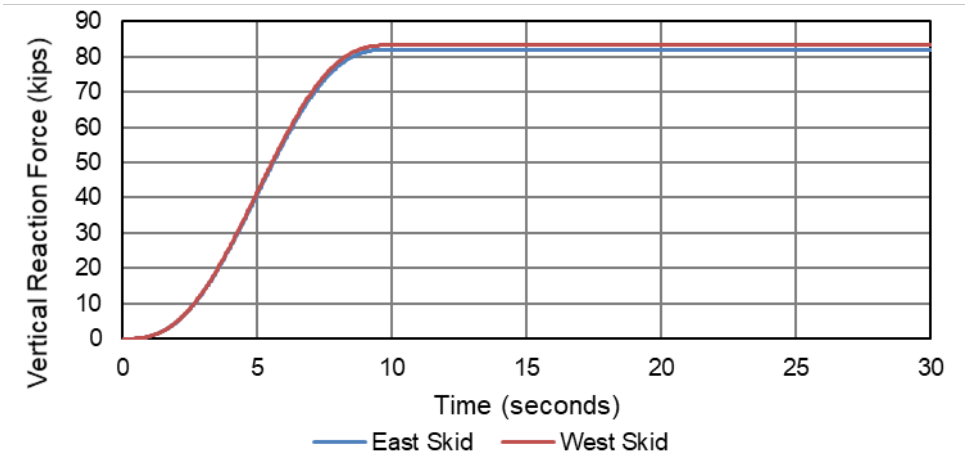

Figure 5. Vertical Reaction Force at Skids

The initial length of the inner vessel was approximately 520 inches, and it was reduced by ~0.32 percent due to thermal contraction at steady state. The initial diameter of the inner vessel was approximately 100 inches and it was reduced by ~0.29 percent due to thermal contraction at steady state.

Figure 6 shows the reduction in volume of the inner vessel. The volume of the inner vessel was measured using a fluid cavity definition in Abaqus so that the volume could be easily requested. The fluid cavity had an initial pressure of 0 psia which remained constant throughout the analysis and did not affect the stress-state of the DOT-113 surrogate. An analogous technique was used to represent a tensile coupon extensometer in models of steel tensile specimens with a soft spring. A reduction in volume of ~1 percent was measured after 45 seconds.

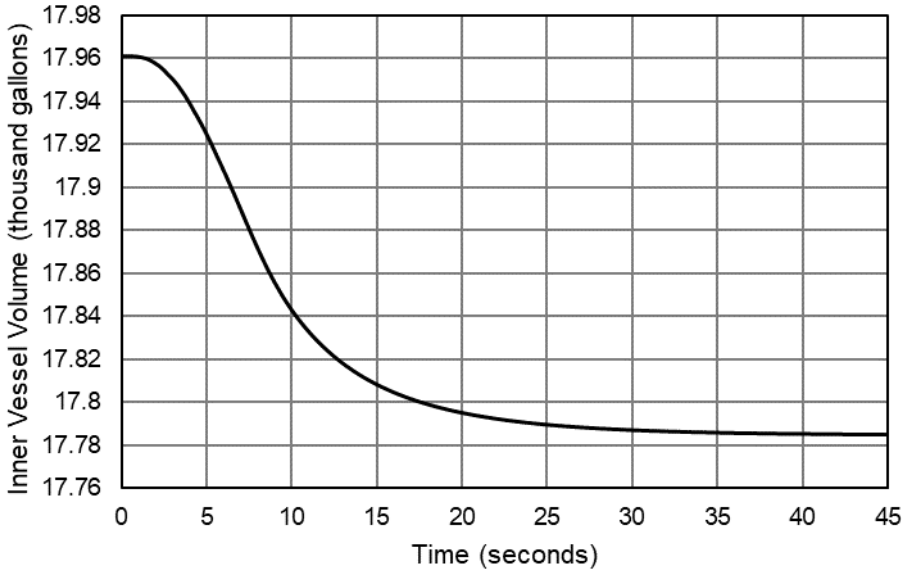

Figure 6. Inner Vessel Volume vs. Time

Figure 7 shows a contour plot of the von Mises stress on a view of the inner vessel. The average von Mises stress on the shell of the inner vessel was ~5 ksi due to thermal contraction and pressurization.

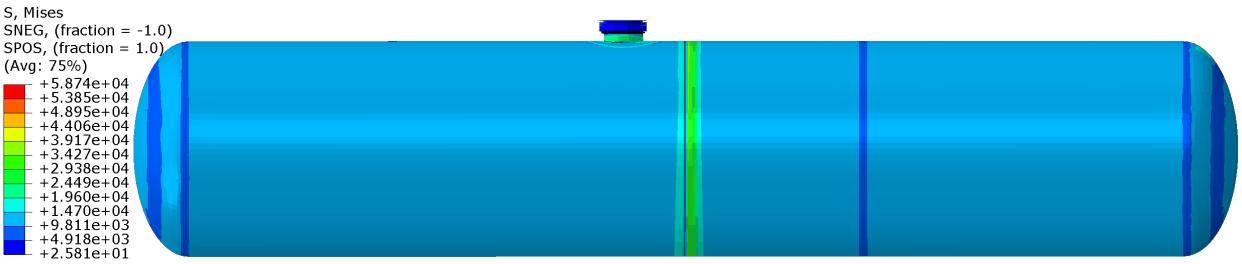

Figure 7. Contour Plot of von Mises Stress (psi)

The results of the coupled thermal-stress analysis indicate that the changes to the geometry and stress state of the DOT-113 surrogate due to loading from thermal contraction, gravity, vacuum, and pressurization are far below what is expected due to loading from the side impact test. For the sake of simplicity and computational efficiency, the initial loading of the DOT-113 surrogate due to gravity and thermal contraction are neglected in the analyses presented in Section 3.3 and Section 4.5. This means that the inner vessel is initially at a cryogenic temperature. Table 5 summarizes the initial conditions included or excluded from the DOT-113 surrogate in the side impact puncture FE model.

Table 5. Initial Conditions Included or Excluded from the Side Impact FE Model

Physical Property	**Included / Excluded**
Gravity	Excluded
Thermal Contraction	Excluded
Vacuum	Included
Internal Pressure	Included

In summary, gravity and thermal contraction were excluded because it was observed that a computationally intensive settling time would be needed to reach steady-state while pressurization of the inner tank and depressurization of the annular space did not require a settling period. Additionally, the initial stresses resulting from gravity loading and thermal contraction were negligible.

3. Gaseous Nitrogen

The FE models developed in support of this test included a representation of the LN2 partially-filling the tank, and the pressurized N2 gas in the outage space. While the gaseous N2 in the outage was at a combination of temperature and pressure that allowed it to initially exist in the gas phase, there were several uncertainties associated with N2 gas at a temperature that was only slightly above that of the LN2 filling the tank. Pre-test exploration of these issues was conducted using simplified mathematical models and simplified FE models. The uncertainties associated with modeling the gas phase in this test and how they were addressed in the pre-test models are described in this section.

Using pressurized N2 gas at a cryogenic temperature introduced several new behaviors that were previously considered negligible when testing using air at ambient temperature. Table 6 summarizes the three behaviors and sections that discuss their treatment.

Table 6. Summary of Sections on Gaseous Nitrogen

Behavior	Theory Section	Modeling Section
Adiabatic heating	3.1	3.3.1
Phase change (i.e. condensing) of gas into liquid	3.1.1	3.3.2
Non-negligible intermolecular forces and volume occupied by gas molecules	3.2	3.3.3

3.1 Thermodynamics

When a gas expands or contracts there is a corresponding change in temperature due to *adiabatic* cooling or heating, respectively. In a FEA, the change in volume of a gas can be modeled with or without adiabatic heating effects. If adiabatic heating effects are excluded and the gas is kept at a constant temperature then the process is considered to be *isothermal*. This typically corresponds to a slow process where heat energy transfer (Q) with the surroundings is faster than heat is generated by work (W). Conversely, if adiabatic heating effects are included then it is assumed that heat is generated at a rate faster than heat is exchanged with the surroundings. Equation 1 shows the first law of thermodynamics for a closed system, i.e., no mass flow, describing the change in internal energy (ΔU).

Equation 1. First Law of Thermodynamics for a Closed System

$$\Delta U = Q - W$$

The *internal energy* of a thermodynamic system is defined as the energy contained within it, i.e., the energy required to create or prepare the system in its given state. Internal energy does not include the kinetic energy motion of the whole system, i.e., gross movement of the entire gas, or the potential energy of the system due to external forces or fields (e.g., gravity). The exclusion of potential energy also means that the energy required to create space for the system by displacing its surroundings is not included.

Table 7 describes the different types of thermodynamic processes and simplifications that can be made for ideal gases. Table 8 summarizes the types of thermodynamic interactions between systems.

Table 7. Types of Thermodynamic Processes

Adiabatic	no transfer of heat or mass with surroundings $Q = 0, \Delta U = -W$
Isothermal	constant temperature, no change in internal energy for an ideal gas $\Delta T = 0$, For an ideal gas: $\Delta U = 0$ and $Q = W$
Isochoric	constant volume, no change in work $\Delta V = 0, W = 0$
Isobaric	constant pressure $\Delta p = 0$
Isoentropic	adiabatic and reversible For an ideal gas: $pV^{\gamma} = constant$

Table 8. Types of Interactions Between Thermodynamic Systems

Type of System	Mass Flow	Work	Heat
Open	Yes	Yes	Yes
Closed	No	Yes	Yes
Thermally isolated	No	Yes	No
Mechanically isolated	No	No	Yes
Isolated	No	No	No

For dynamic impact events involving gas expansion/compression, the expansion/compression of the gas is typically modeled as either (1) a *thermally isolated* system in which the heat energy transfer with its surroundings is approximately zero or (2) an *isothermal* thermodynamic process where a constant temperature is maintained by transferring heat with its surroundings. For very fast events, a thermally isolated system is typically considered while slower dynamic events can be considered isothermal. Previous modeling experience of tank car side impact tests has indicated that an isothermal assumption results in reasonable agreement between the models and tests.

The internal energy per unit mass (m), i.e., specific internal energy (u), of an ideal gas is proportional to its absolute temperature per Equation 2 where c_v is the specific heat at constant volume and u_0 is the initial specific energy. The specific heat at constant volume is used to describe internal energy because internal energy does not include the work done to make space (volume) for the system by displacing its surroundings.

Equation 2. Specific Internal Energy of an Ideal Gas

$$u = \frac{U}{m}$$

$$u(\theta) = u_0 + \int_{\theta_0}^{\theta} c_v(T)\, dT$$

Enthalpy (H) is defined as the internal energy plus the product of its pressure and volume. Enthalpy is a state function that describes the internal energy of a system plus the work required to make room for the system when displacing its surroundings. When considering the work done to make room for the system, the specific heat at constant pressure (c_p) is used. Specific enthalpy (h) is the enthalpy per unit mass. For an ideal gas, enthalpy is independent of pressure and only depends on temperature per Equation 3.

Equation 3. Change in Specific Enthalpy for an Ideal Gas

$$\boldsymbol{H = U + pV}$$

$$h = \frac{H}{m}$$

$$h(\theta) = h_0 + \int_{\theta_0}^{\theta} c_p(T)\, dT$$

While Equation 1 describes the first law of thermodynamics for a closed system, mass transfer can be considered for an open system by balancing the first law of thermodynamics, which Equation 4 shows can be written in terms of specific energy.

Equation 4. First Law of Thermodynamics for an Open System

$$\frac{d\,(m \cdot u)}{dt} = \frac{dQ}{dt} - \frac{dW}{dt} + h_{in}\frac{dm_{in}}{dt} - h_{out}\frac{dm_{out}}{dt}$$

$$m_{in} = mass\ flow\ into\ the\ system$$

$$m_{out} = mass\ flow\ out\ the\ system$$

$$h_{in} = specific\ enthalpy\ of\ m_{in}$$

$$h_{in} = specific\ enthalpy\ of\ m_{out}$$

$$\frac{dW}{dt} = p\frac{dV}{dt} = instantaneous\ work\ done\ by\ ideal\ gas\ expansion$$

$$\frac{dQ}{dt} = instantaneous\ heat\ energy\ flow\ rate\ into\ surroundings$$

The specific gas constant (R) is equal to the universal gas constant divided by the molecular weight (MW). Equation 5 defines the specific gas constant and ratio of heat capacities (γ).

Equation 5. Specific Gas Constant and Ratio of Heat Capacities

$$R = \frac{Ru}{MW}$$

$$R = c_p - c_v$$

$$\Upsilon = \frac{c_p}{c_v}$$

A polytropic relationship can be used to describe the relationship in many expansion and compression thermodynamic processes. Equation 6 describes a polytropic process where n is defined as the polytropic index.

Equation 6. Polytropic Process Relationship

$$pV^n = constant$$

Table 9 summarizes the different types of polytropic thermodynamic processes.

Table 9. Description of Different Polytropic Thermodynamic Processes

$n < 0$	A negative exponent corresponds to a spontaneous process where thermodynamic interactions are not dominant, such as an explosion
$n = 0$	Isobaric process (constant pressure) $p = constant$
$n = 1$	Isothermal process (constant temperature) $pV = constant$
$1 < n < \gamma$	Heat and work flows go in opposite directions, such as in vapor compression refrigeration
$n = \gamma$	Isoentropic process (adiabatic and reversible)
$\gamma < n < +\infty$	Heat and work flows go in the same direction, such as in an internal combustion engine
$n = +\infty$	Isochoric process (constant volume) $V = constant$

3.1.1 Phase Change

The enthalpy of vaporization (ΔH_{vap}) is the amount of energy that must be added to a liquid to transform it into a gas. It is often referred to as latent heat and can be written as a function of pressure or temperature. It can be considered as the energy required to cross the saturation curve shown in Figure 8. Equation 7 gives the enthalpy of vaporization in terms of the change in internal energy of the gas and liquid phases (ΔU_{vap}) plus the work done on the surroundings. When changing from gas to vapor, ΔU_{vap} can be considered the work needed to overcome the

intermolecular forces of the liquid phase; in the case of LN2, these intermolecular forces are van der Waals forces—more specifically London dispersion forces.

Equation 7. Enthalpy of Vaporization

$$\Delta H_{vap} = \Delta U_{vap} + p\Delta V$$

3.2 Ideal and Real Gas Equations of State

An ideal gas is a theoretical gas containing molecules moving randomly that are not subject to inter-particle forces. The ideal gas model has two assumptions:

(1) Intermolecular forces, e.g., van der Waals forces, are neglected

(2) The volume occupied by a gas molecule is neglected

The ideal gas model is typically not applicable at very low temperatures or high pressures where the molecular size and intermolecular forces can affect the random motion of molecules.

The ideal gas law is an equation of state (EOS) given in terms of absolute pressure (p), volume (V), number of moles (n), universal gas constant (R_u), and absolute temperature (T). To consider attractive forces between the molecules of a real gas, a compressibility factor (Z) can be incorporated to describe the deviation as shown in Equation 8.

Equation 8. Ideal Gas Law and Definition of Compressibility Factor

$$pV = nR_uT$$

$$pV = ZnR_uT$$

The compressibility factor is dependent on temperature and molar volume (V_m) or pressure. The Virial expansion can be used to describe the compressibility factor at a molecular level based on statistical mechanics [8]. The Virial equation is shown in Equation 9 where each term of the Virial expansion describes the interactions between successively larger groups of molecules. The coefficient $B(T)$ accounts for interactions between two molecules, the coefficient $C(T)$ accounts for interactions between three molecules, and so forth.

Equation 9. Virial Equation for Compressibility Factor

$$Z = 1 + \frac{B(T)}{V_m} + \frac{C(T)}{V_m} + \frac{D(T)}{V_m} +$$

When the compressibility factor is less than 1, attractive forces dominate the interaction. When the compressibility factor is greater than 1, repulsive forces dominate the interaction. At cryogenic temperatures, the compressibility factor is typically less than 1 because van der Waals forces result in a significant attractive force. This attractive force causes a gas to behave more like a liquid.

Figure 8 shows the saturation curve of nitrogen based on Antoine Equation coefficients calculated by the National Institute of Standards and Technology (NIST) using test data from Edejer and Thodos (1967). For comparison, the targeted initial pressure and the settings for the pressure relief valves (PRV) including the first start-to-discharge pressure (STDP #1) and second start-to-discharge pressure (STDP #2) for the DOT-113 surrogate are also shown. At the targeted initial outage pressure of 62.3 psia the saturation temperature (i.e., boiling point) is approximately 92 K. A uniform initial pressure and temperature of 62.3 psia and 92 K were

assumed for the entire outage. For combinations of pressure and temperature that are above or to the left of the saturation curve, the nitrogen will be in a liquid state. For combinations of pressure and temperature that are below or to the right of the saturation curve, the nitrogen exists as a gas.

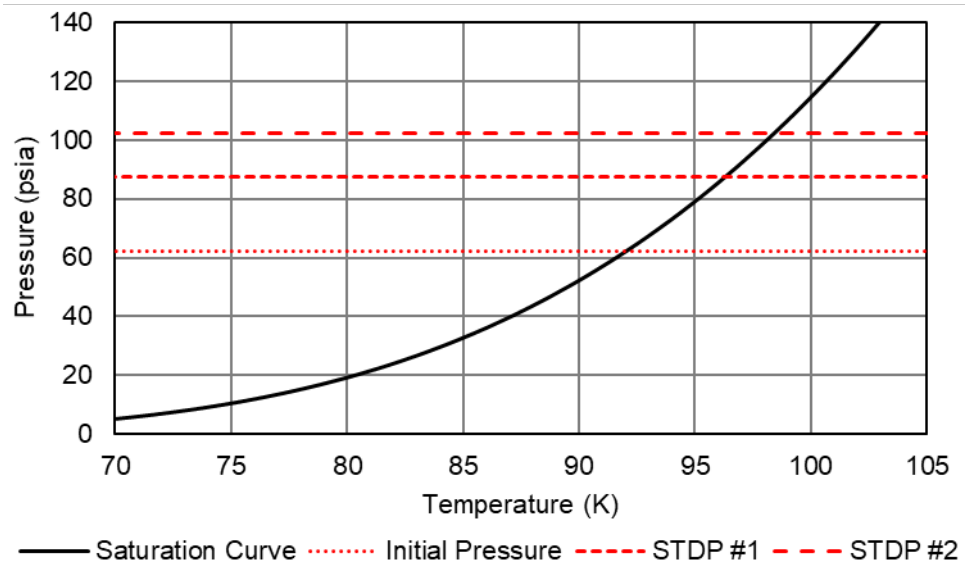

Figure 8. Saturation Curve of Nitrogen

Table 10 shows the properties of nitrogen from the NIST Standard Reference Database 69: *NIST Chemistry WebBook*. Because the predicted temperature and pressure of the nitrogen gas in the outage is well below the critical temperature (T_c) and critical pressure (p_c), it can be assumed that van der Waals forces play a significant role in the compressibility of the gas and the ideal gas law does not apply, i.e., the compressibility factor is much less than 1.

Table 10. Properties of Nitrogen

Property	Value (FE Model Units)	Value (SI Units)
Molecular Weight	1.599606E-04 lbf-s^2/(mol-in)	28.0134 g/mol
Specific Gas Constant	460037.9803 in^2/(K-s^2)	0.296797961 J/(g-K)
Critical temperature (T_c)	126.192 K	-
Critical pressure (p_c)	492.52 psia	3.3958 MPa
Critical density (D_c)	0.183271 mol/in^3	11.1839 mol/L
Acentric factor	0.0372	-
Normal boiling point	77.355 K	-

3.2.1 Redlich-Kwong Equation of State

The Redlich-Kwong EOS is an empirical modification of the ideal gas EOS intended to account for the attractive potential of molecules and the volume of molecules with the parameters *a* and

b, respectively [9]. The Redlich-Kwong EOS for a real gas and determination of *a* and *b* are shown in Equation 10.

Equation 10. Redlich-Kwong Equation of State for a Real Gas

$$R_u T = \left(p + \frac{a}{\sqrt{T} V_m (V_m + b)}\right)(V_m - b)$$

$$p = \frac{R_u T}{(V_m - b)} - \left(\frac{a}{\sqrt{T} V_m (V_m + b)}\right)$$

$$a = 0.42748 \frac{R_u{}^2 T_c^{5/2}}{p_c}$$

$$b = 0.08664 \frac{R_u T_c}{p_c}$$

Table 11 contains the Redlich-Kwong parameters *a* and *b* for N2 using the properties from Table 10 and Equation 10.

Table 11. Redlich-Kwong Parameters for Nitrogen

a	***b***
lbf-K$^{1/2}$/mol	*in^3/mol*
8.4078E+05	1.6336

3.3 Modeling Gas Behavior

Appendix A contains a description of the non-puncture FE model used to investigate the gas behavior. The exclusion of very small solid elements which are necessary to simulate puncture allowed for the non-puncture model to run to completion approximately eight times faster. This allowed for a variety of gas modeling techniques to be applied to separately investigate the effects of: (1) adiabatic heating, (2) phase change, and (3) real gas compressibility. For Section 3.3.1, a similar non-puncture version of the Test 11 DOT-113 surrogate (i.e., filled with water and air) was also used.

The effects of adiabatic heating, phase change, and real gas compressibility were not combined in a single model because it would require (1) detailed modeling of heat transfer of the gas phase with its surrounding and (2) complex functionality that is not available in Abaqus/Explicit without custom user subroutines. Considering the effects separately still enabled the authors to consider their effects on the pre-test estimate of puncture speed to book-end the expected response of the DOT-113 surrogate.

3.3.1 Adiabatic Heating Modeling

In Abaqus/Explicit, the outage of the DOT-113 surrogate tank car from Test 11 was represented as a pneumatic cavity. An ideal gas EOS was used for air at room temperature since the initial pressure (62.3 psia) is well below air's critical pressure, and the initial temperature (294 K) is well above its critical temperature. In Abaqus/Explicit, adiabatic heating effects can be included or excluded from the simulation. If adiabatic heating effects are excluded, then the compression

of the outage is an isothermal process, i.e., constant temperature. If adiabatic heating effects are included, then the compression of the outage is considered an isoentropic thermodynamic process, i.e., the outage gets hotter as it is compressed, and heat flux out of the outage is neglected. Allowing the outage to increase in temperature when the volume is reduced, which further increases the pressure due to the ideal gas EOS.

Two non-puncture FE models of the Test 11 conditions were executed using the isothermal and adiabatic assumptions. The pressure time-history outputs from the FE models using the two assumptions are shown in Figure 9 with the actual test results from two pressure transducers in the outage (i.e., TP1000, TP3000) plotted for comparison. Even though the pressure rises rapidly over a period of 0.3 seconds, the isothermal assumption shows better agreement between the FE model and the test results. This indicates that heat is rapidly exchanged with the stainless steel tank and water which enclose the outage.

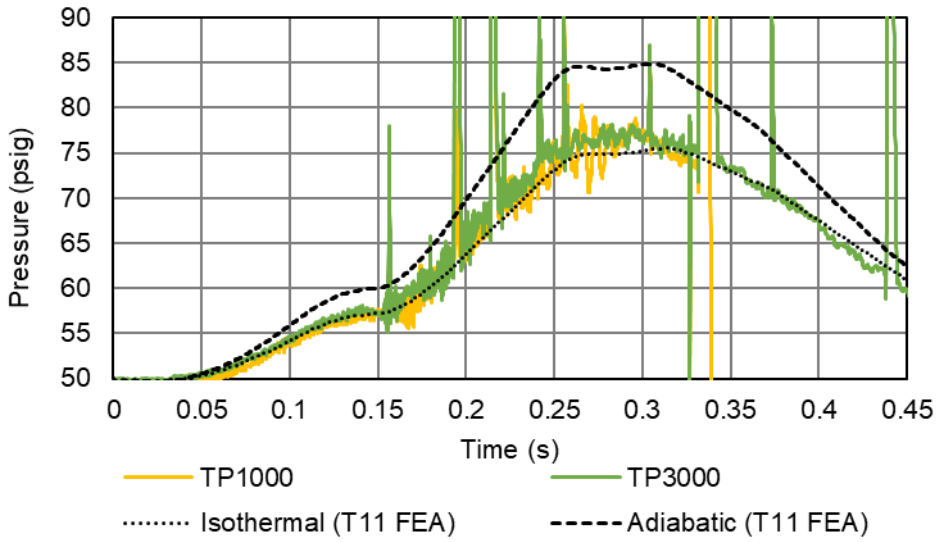

Figure 9. Comparison of Outage Thermodynamic Processes in Test 11 Simulation

While the isothermal assumption has resulted in good agreement with previous side impact FEA with room temperature water and air, it was unclear if the same assumption would yield accurate model results with cryogenic nitrogen and a well-insulated tank. To address this, a non-puncture model of the DOT-113 surrogate tank car filled to 95 percent with LN2 and pressurized to 50 psig with N2 was run at 18 mph with isothermal and adiabatic ideal gas assumptions. Because the N2 started on its saturation curve at 62.3 psia and 92 K, any increase in pressure without an accompanying increase in temperature would result in condensation; however, condensation was not considered to simplify the analysis. In the isothermal case, heat transfer between the gaseous N2 and its surroundings was assumed to be infinite so that any adiabatic heat generated during compression was transferred to the surroundings and could be neglected during the analysis. In the adiabatic case, heat transfer from the gaseous N2 was assumed to be zero so that all adiabatic heat generated during compression increased the temperature of the gas.

Figure 10 shows temperature versus time for the isothermal and adiabatic ideal gas models. The isothermal model maintained a constant temperature of 92 K, while the adiabatic model achieved a peak temperature of 128 K i.e., an increase of 36 K. The saturation temperature for each model is plotted for comparison and calculated using the pressure time history output from the models

(Figure 11). The adiabatic model does not cross the adiabatic saturation curve which indicates that a phase change is unlikely to occur assuming that no generated heat leaves the gas. The isothermal model crosses the isothermal saturation curve indicating that a phase change is likely to occur if heat quickly transfers out of the gas during compression. The results indicate that the rate of heat flux out of the N2 gas (i.e., Q in Equation 1) will determine whether or not a phase change would occur.

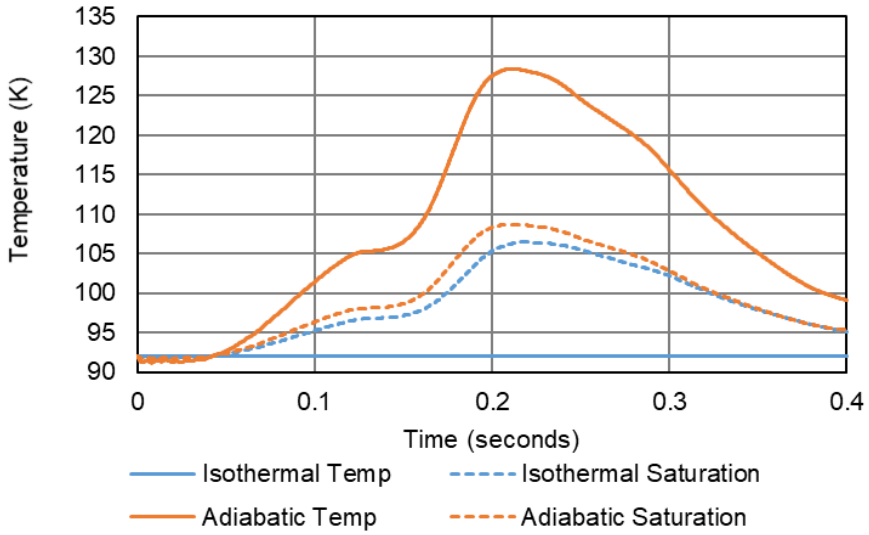

Figure 10. Temperature vs. Time for Isothermal and Adiabatic Ideal Gas Assumptions

Figure 11 shows pressure versus time for the isothermal and adiabatic ideal gas models. In the isothermal case, the relationship between pressure and volume is $pV = constant$ and in the adiabatic case the relationship between pressure and volume is $pV^n = constant$ where n is equal to γ (i.e., defined in Equation 6) and is always greater than 1. By allowing temperature to increase, a corresponding reduction in volume results in a larger increase in pressure in the adiabatic case versus isothermal case.

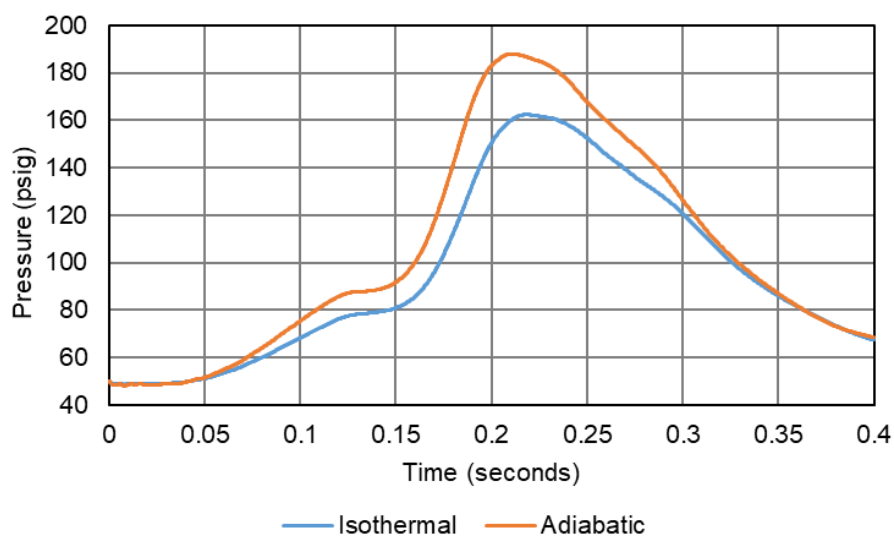

Figure 11. Pressure vs. Time for Isothermal and Adiabatic Ideal Gas Assumptions

Figure 12 shows impactor force versus travel for the isothermal and adiabatic ideal gas models. Even though the adiabatic model reaches a peak pressure that is 16 percent higher than the isothermal model, the resulting peak impactor force only increased by 5 percent and impactor travel only decreased by 2 percent.

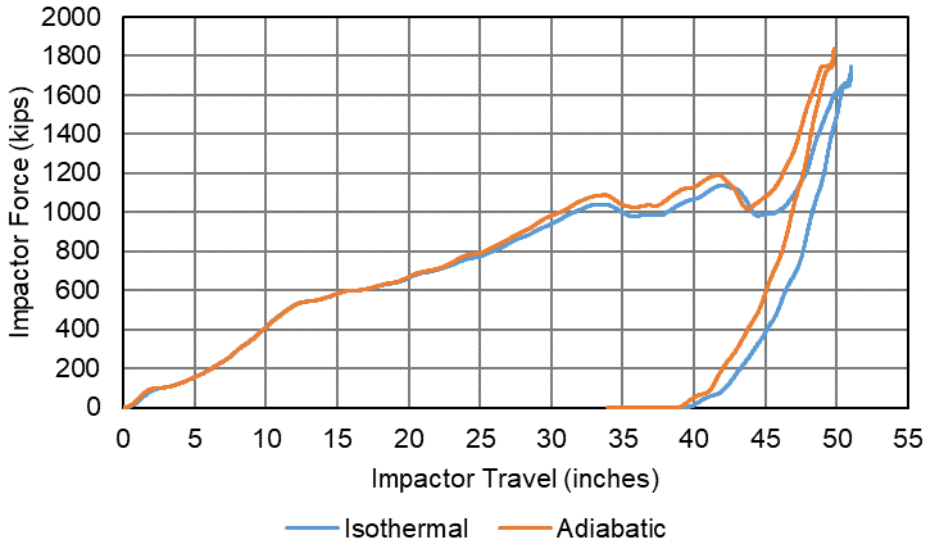

Figure 12. Impactor Force vs. Travel for Isothermal and Adiabatic Ideal Gas Assumptions

Both the isothermal and adiabatic results presented in this section neglect the compressibility of a real gas and do not consider phase change. Because of the complexities and potential instability of modeling the simultaneous effects of heat transfer, real gas compressibility, and phase change, these effects were modeled separately. The subsequent sections discuss modeling of N2 with isobaric phase change and as an isothermal real gas.

3.3.2 Phase Change Modeling

In previous tank car tests using air at atmospheric or elevated pressure and ambient temperature, the gas in the outage could be correctly assumed to remain a gas for the duration of the impact event. This simplified modeling the outage in those tests, as the ideal gas law was applicable without additional considerations. For Test 12, the gaseous N2 in the outage was initially at a pressure of 62.3 psia. At this pressure, the saturation temperature was approximately 92 K. An increase in pressure also results in an increase in the saturation temperature (i.e., the saturation curve in Figure 8). If the temperature of the gas were below the saturation temperature at any given pressure, the gas could experience a phase change by condensing into a liquid. A phase change could also occur if the pressure of the gas remained the same but the temperature of the gas dropped below the saturation temperature.

A simple solution would be to keep the gas at a temperature that is much higher than the saturation temperature at the initial pressure of 62.3 psia. An elevated temperature of the gas would require a more substantial decrease in temperature or increase in pressure to cross the saturation curve. However, it is not necessarily possible to maintain equilibrium between the gas and LN2 with such a large difference in temperature, as the LN2 must be kept *below* the saturation temperature at a given pressure to remain in the liquid state.

Assuming that gaseous nitrogen is initially at its saturation temperature and that its temperature remains constant, the process of compressing the gas should be isobaric (constant pressure). Conversely, if it is assumed that temperature remains constant and no phase change occurs, the gas would be beyond its condensation point.

Figure 13 shows pressure versus time for the isothermal ideal gas and isobaric phase change models. The isothermal ideal gas behavior is the same as what was presented in Section 3.3.1 and the isobaric behavior was simulated as a constant pressure load applied to the inner surface of the membrane surrounding the outage's pneumatic cavity. Thus, the ability of the outage to build pressure was suppressed.

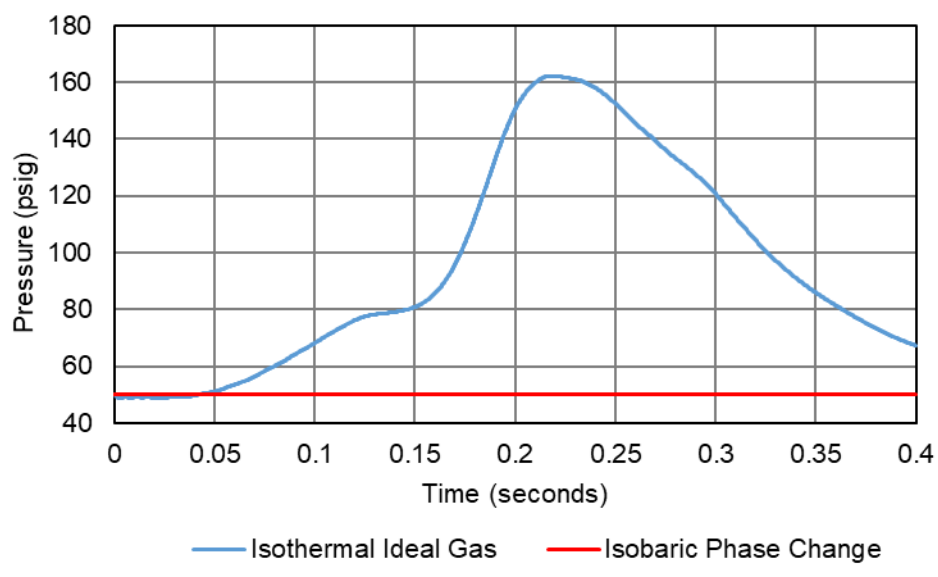

Figure 13. Pressure vs. Time for Isothermal Ideal Gas and Isobaric Phase Change Models

Figure 14 shows outage volume versus time for the isothermal ideal gas and isobaric phase change models. The volume of the gas is reduced by more than 50 percent in the isothermal case and by nearly 100 percent in the isobaric case. This indicates that if heat is able to quickly leave the gas phase, the external work done to compress the gas by the impactor at 18 mph would be sufficient to condense nearly all the gas to liquid.

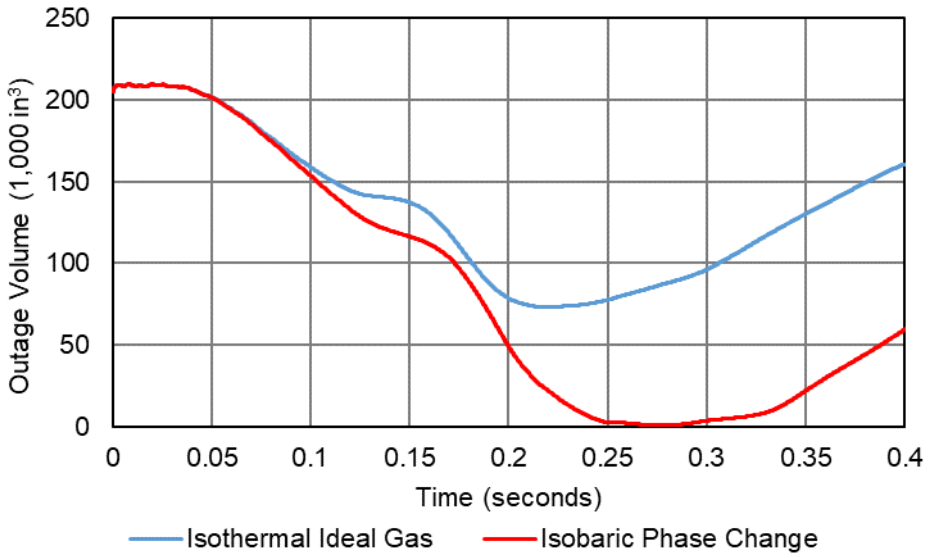

Figure 14. Outage Volume vs. Time for Isothermal Ideal Gas and Isobaric Phase Change Models

Figure 15 shows impactor force versus travel for the isothermal ideal gas and isobaric phase change models, both run at 18 mph. While the adiabatic model did not show a large difference from the isothermal model in force versus travel, the isobaric model shows a clear change. In the isobaric case, the peak impactor force was reduced while the peak impactor travel increased.

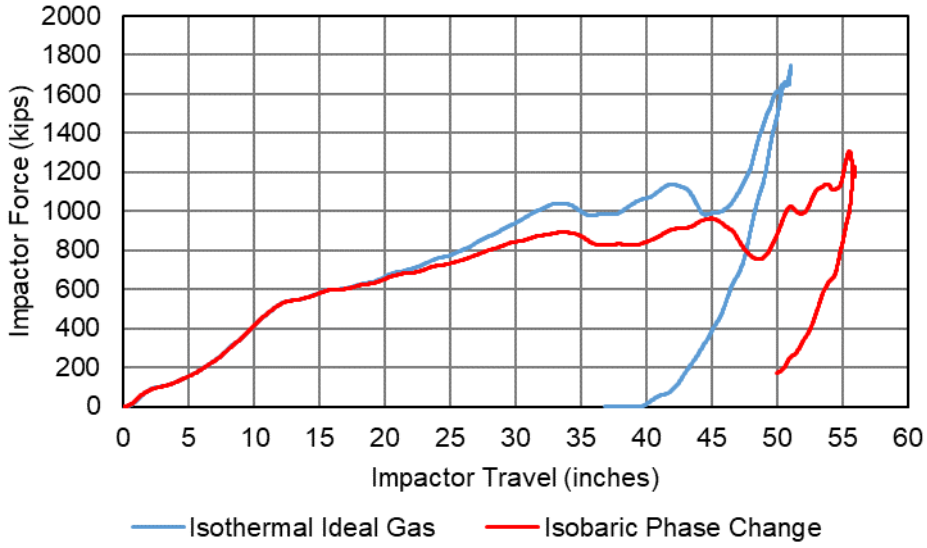

Figure 15. Impactor Force vs. Travel for Isothermal Ideal Gas and Isobaric Phase Change Models

3.3.3 Real Gas Modeling

Because the outage is initially below the critical temperature and pressure, the outage should behave like a real (non-ideal) gas. This means that the ideal gas EOS should over-predict a change in pressure corresponding to a given change in volume.

Abaqus/Explicit does not include a built-in functionality for modeling a real (i.e., non-ideal) gas using the pneumatic cavity approach (e.g., uniform pressure method). Due to this limitation, the model was run iteratively to estimate the compressibility of an isothermal real gas.

1. The FE model was first run using an ideal gas EOS in a pneumatic cavity representing the outage with an isothermal assumption. Afterwards the pneumatic cavity was suppressed for further iterative runs so that changes in outage volume were not directly used to calculate pressure changes at each time increment.
2. The volume time-history from the isothermal model was post-processed and used to estimate a pressure time history with the Redlich-Kwong EOS given in Equation 10.
3. The post-processed Redlich-Kwong pressure-time history was then used as an input pressure-time history acting on the membrane surrounding the outage in the next model run.
4. The new volume time history was again post-processed to calculate a new pressure time history with the Redlich-Kwong EOS.
5. This process was repeated until the volume time history no longer changed substantially between runs.

Because the model was first run with the pneumatic cavity having an ideal gas EOS, the corresponding change in volume in the outage was smaller than if the model was run with the Redlich-Kwong EOS. The model had to be run iteratively to achieve an output volume time history that correctly corresponded to the input Redlich-Kwong pressure time history.

Figure 16 shows the outage volume time history from the non-puncture model iterations. The first model with an ideal gas (i.e., light blue curve) had the smallest reduction in volume. The next model named Redlich-Kwong #1 (i.e., orange curve) had the largest reduction in volume because the volume-time history from the ideal gas model underestimated the pressure-time history in the first iteration of the Redlich-Kwong EOS. Subsequent iterations oscillated up and down in volume reduction until a steady state was reached after approximately 5 iterations; at which point, the simulations were stopped.

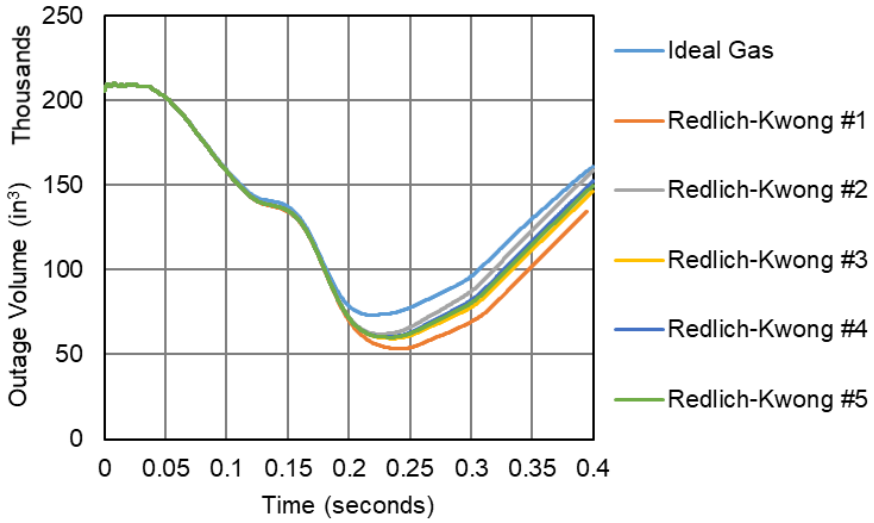

Figure 16. Outage Volume Time History

Figure 17 shows the outage pressure-time history from the non-puncture model. The pressure time history also shows that steady state was achieved after approximately five iterations. Each Redlich-Kwong pressure time history was calculated using the previous iteration's volume time history; i.e., the curve named *Redlich-Kwong #2* in Figure 17 was calculated using the volume time history named *Redlich-Kwong #1* in Figure 16. Using this iterative approach peak pressure was reduced from 162 psig with the ideal gas EOS to 138 psig with the converged Redlich-Kwong EOS.

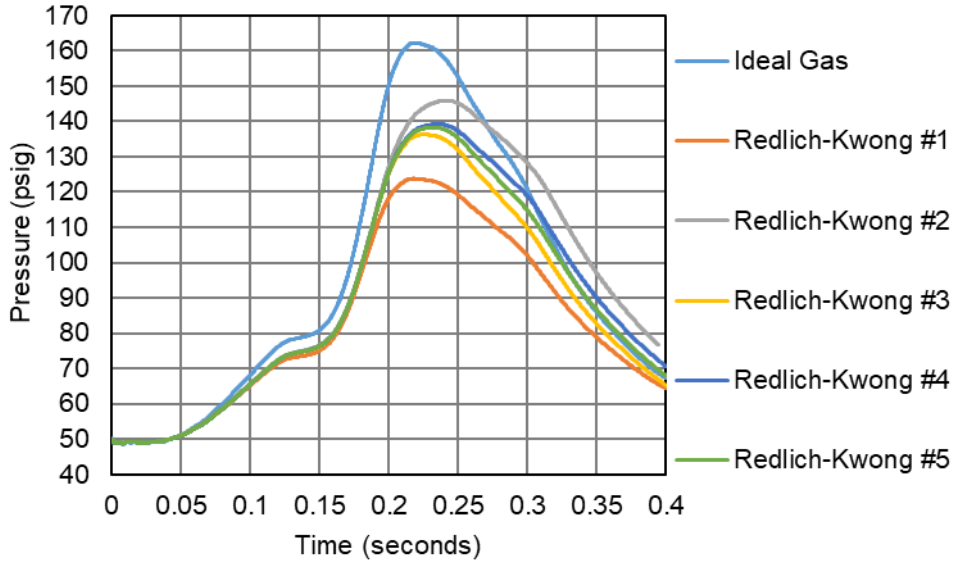

Figure 17. Outage Pressure Time History

Figure 18 shows the corresponding impactor force versus travel responses for the non-puncture model. The Redlich-Kwong model results were omitted prior to convergence as there was not a large amount of variation in the force-travel response. In looking at the ideal gas EOS versus Redlich-Kwong EOS results, it is clear that the force-travel responses are similar. The Redlich-Kwong converged results exhibited a slightly decreased peak force and a slightly increased peak indentation compared to the ideal gas model result. Based on this, it is expected that the threshold puncture speeds would be similar in a puncture FE model; however, this iterative approach may be a challenge to implement using a puncture-capable FE model due to runtime and stability concerns.

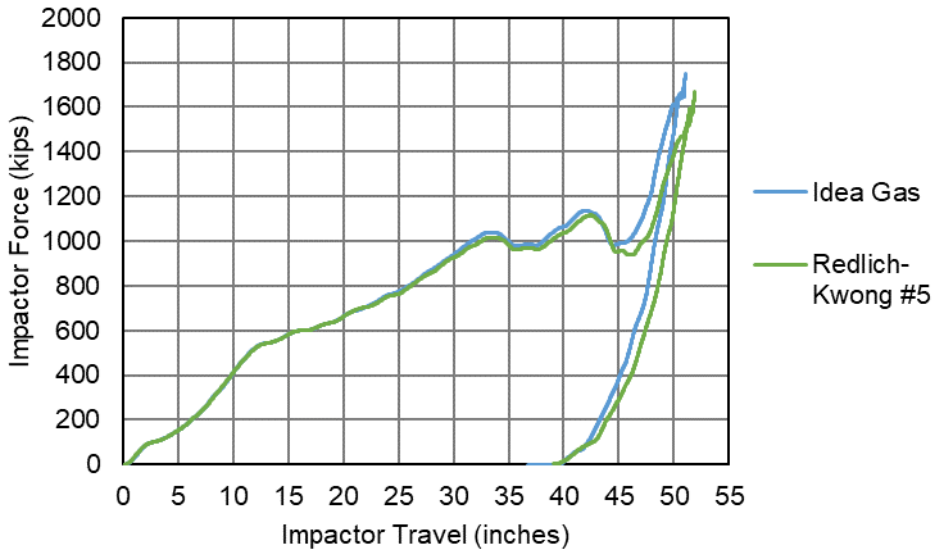

Figure 18. Impactor Force vs. Travel

Unfortunately, Abaqus/Explicit does not currently support custom user subroutines for a pneumatic cavity. Thus, the Redlich-Kwong EOS cannot be directly implemented in Abaqus/Explicit, even with a user subroutine. Abaqus/Explicit does support the use of a user subroutine to define a conventional material, which could then be defined in a Lagrangian or Eulerian mesh, or with the smoothed particle hydrodynamics (SPH) approach. However, any of these techniques for representing the outage would be computationally expensive compared to the fluid cavity approach. Additionally, implementation of a user material for the Redlich-Kwong EOS and a meshed or SPH representation of the gas could potentially result in model instabilities.

In summary, a simplified iterative process was developed to apply the Redlich-Kwong EOS to the Abaqus/Explicit model using an isothermal pneumatic cavity for the outage. As described above, the non-puncture FE model was first run using an ideal gas EOS pneumatic cavity. The volume-time history was requested from this cavity and used to post-process a pressure-time history using the Redlich-Kwong EOS outside of Abaqus. The FE model was then modified to replace the ideal gas pneumatic cavity with a cavity having a prescribed pressure-time history based on the output from the Redlich-Kwong EOS. The FE model with the prescribed pressure-time history was run and the volume-time history of the outage was requested as output. This volume-time history was then used to estimate a pressure-time history using the Redlich-Kwong EOS.

3.3.4 Summary of Gas Modeling

An isothermal ideal gas assumption has been used in modeling the recent tank car side impact tests with water. As the planned Test 12 is the first test to use a cryogenic lading, the validity of an ideal gas assumption was reexamined. Table 12 summarizes the effect that various modeling assumptions have on the overall behavior of the non-puncture FE model. The comparisons are made using peak values of increase in gas pressure, decrease in gas volume, increase in gas temperature, increase in impactor force, and increase impactor travel with respect to the baseline

assumption of isothermal ideal gas. The cases that were examined used assumptions of (1) adiabatic ideal gas, (2) isobaric phase change, and (3) isothermal real gas.

Table 12. Gas Modeling Percent Change from Isothermal Ideal Gas

Behavior	Pressure Increase	Volume Decrease	Temperature Increase	Force Increase	Travel Increase
Isothermal Ideal Gas (baseline)	-	-	-	-	-
Adiabatic Ideal Gas	+23%	-22%	+40%	+5%	-2%
Isobaric Phase Change	-100%	+98%	0%	-25%	+10%
Isothermal Real Gas	-21%	+18%	0%	-4%	+2%

These results indicate that if these assumptions were applied to the puncture-capable FE model at an initial pressure of 50 psig, the adiabatic ideal gas would result in the lowest estimate of puncture speed and the isobaric phase change case would result in the highest estimate of puncture speed.

4. LN2

The FE models included a representation of the LN2 partially filling the tank, and the pressurized N2 gas in the outage space. While the LN2 in the tank was at a combination of temperature and pressure that allowed it to initially exist in the liquid phase, there were several uncertainties associated with LN2 that had not previously been encountered in testing using liquid water as the test lading. Pre-test exploration of these issues was conducted using simplified mathematical models and simplified FE models. The uncertainties associated with modeling the liquid phase in this test and how they were addressed in the pre-test models are described in this section.

The temperature dependent LN2 fluid properties were obtained from NIST Standard Reference Database 69: *NIST Chemistry WebBook* at a constant pressure of 62.3 psia [10]. Appendix A, A.4 contains a table of the temperature dependent values fluid properties including dynamic viscosity, density, speed of sound, and bulk modulus. A range of initial temperatures were investigated for LN2 from 77 to 92 K based on the saturation temperature at atmospheric pressure and the targeted test pressure.

4.1 Dynamic viscosity

Figure 19 shows the dynamic viscosity of LN2 at 62.3 psia versus temperature. At the saturation temperature of 92 K, the dynamic viscosity of LN2 is 1.4E-8 psi-s. For the sake of comparison, the dynamic viscosity of water at room temperature is 1.4E-7 psi-s. Since the dynamic viscosity of the lading in Test 12 is an order of magnitude lower than the lading in Test 11, dynamic viscous effects are greatly reduced in the lading's sloshing behavior.

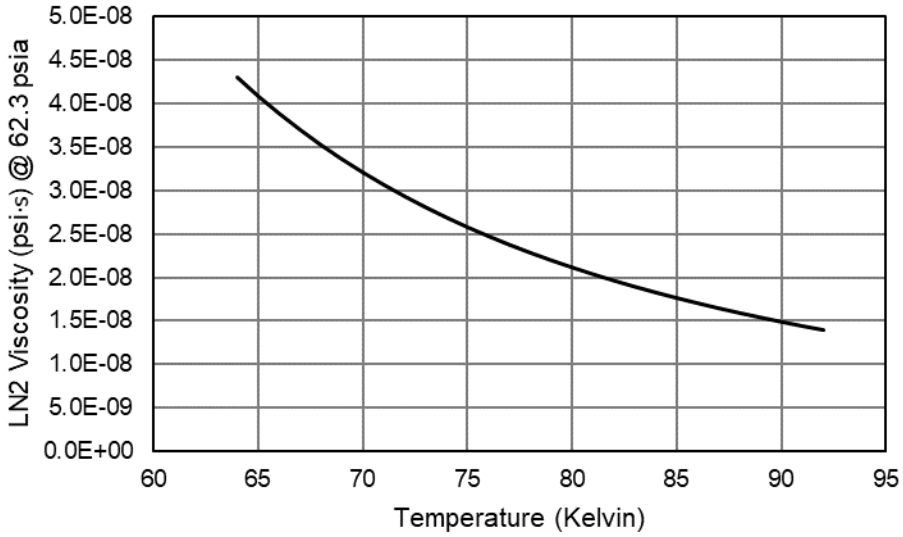

Figure 19. Dynamic Viscosity Properties of LN2 at 62.3 psia vs. Temperature

4.2 Density

Figure 20 shows the density of LN2 at 62.3 psia versus temperature. At the saturation temperature of 92 K, the density of LN2 is 6.9E-05 lbf-s^2/in^4. For the sake of comparison, the density of water at room temperature is 9.3E-05 lbf-s^2/in^4. Since the density of the lading in

Test 12 is 26.4 percent lower than the lading in Test 11, inertial effects are reduced in the lading's sloshing behavior.

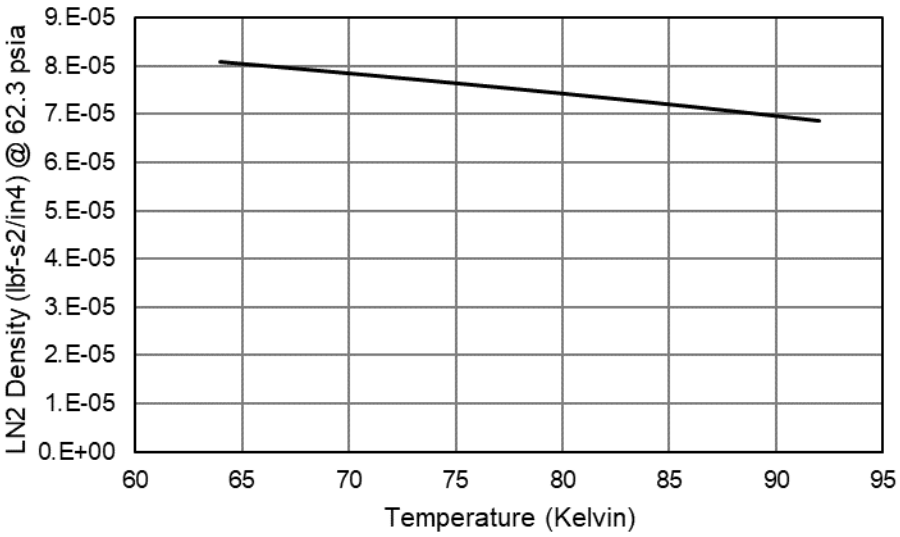

Figure 20. Density of LN2 at 62.3 psia vs. Temperature

4.3 Bulk Modulus

The bulk modulus (K) of a material is a measure of its resistance to compression. In a fluid, the bulk modulus can be calculated from the speed of sound (c) and density (ρ) according to the Newton-Laplace equation given in Equation 11 [11].

Equation 11. Calculation of Bulk Modulus

$$K = c^2\rho$$

Figure 21 shows the bulk modulus of LN2 at 62.3 psia versus temperature. At the saturation temperature of 92 K, the bulk modulus of LN2 is 5.2E+04 psi. For the sake of comparison, the bulk modulus of water at room temperature is 3.2E+05 psi. Since the bulk modulus of the lading in Test 12 is an order of magnitude lower than the lading in Test 11, the lading is more compressible and a softer force-travel response should be expected from the impactor.

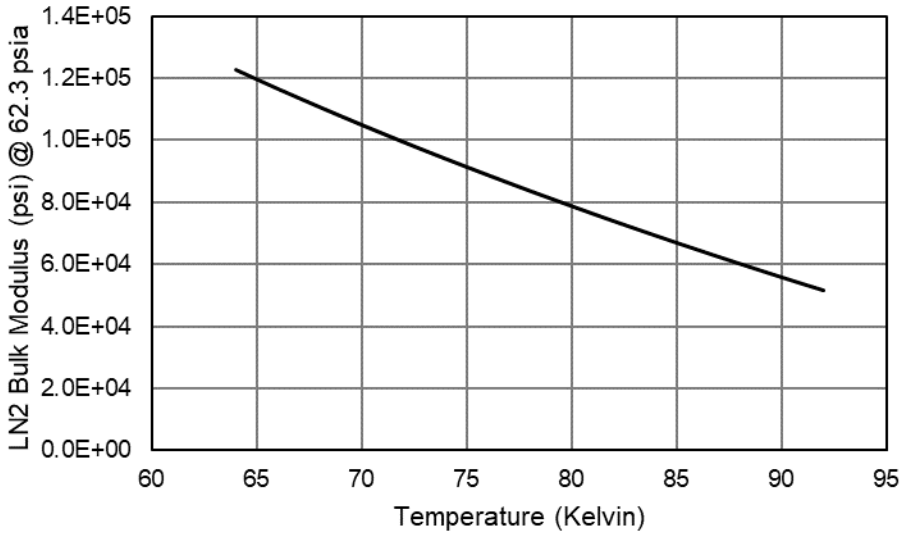

Figure 21. Bulk Modulus of LN2 at 62.3 psia vs. Temperature

4.4 Phase Change

Figure 22 shows the saturation curve of nitrogen based on the Antoine equation coefficients calculated by NIST using test data from Edejer and Thodos (1967). For comparison, the targeted initial pressure and the settings for the PRVs including the first start-to-discharge pressure (STDP #1) and second start-to-discharge pressure (STDP #2) for the DOT-113 surrogate are also shown. At the targeted initial outage pressure of 62.3 psia the saturation temperature (i.e., boiling point) is approximately 92 K. For combinations of pressure and temperature that are above or to the left of the saturation curve, the nitrogen will be in a liquid state. For combinations of pressure and temperature that are below or to the right of the saturation curve, the nitrogen exists as a gas.

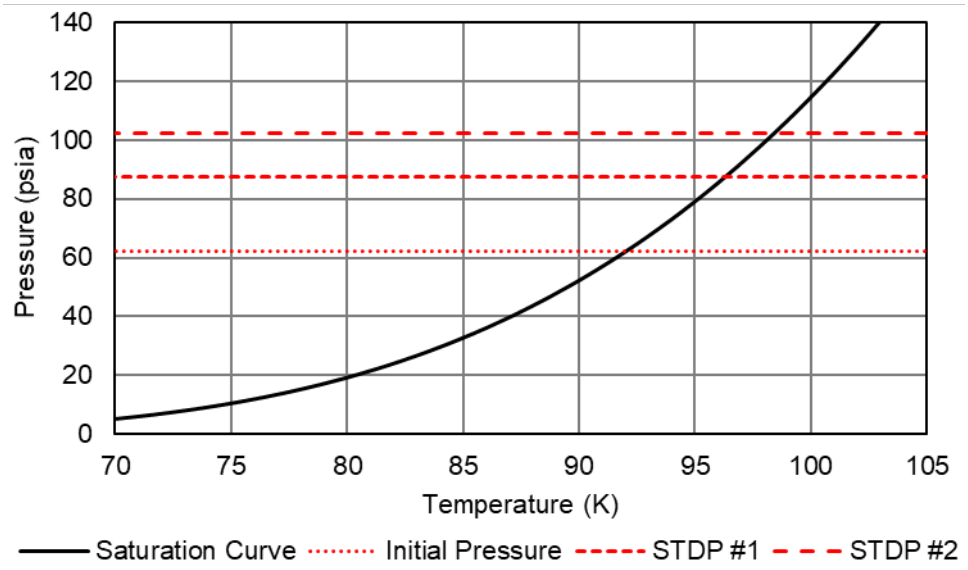

Figure 22. Saturation Curve of Nitrogen

Based on the saturation curve above, for LN2 to exist at the target initial pressure of 62.3 psig the liquid phase could have a temperature no higher than approximately 92 K. However, LN2 can exist in the liquid state at this pressure but a lower temperature. As a lower bound, nitrogen is typically transported at or close to its saturation temperature at atmospheric pressure. This means that the nitrogen used in the test should be no colder than 77 K.

4.5 Summary of Liquid Modeling

The non-puncture FE model shown in Appendix A was used to investigate the difference in the structural response of the DOT-113 surrogate whether it was filled with LN2 at 77 or 92 K. In both cases the initial pressure was 50 psig, the outage was 5 percent, and the initial velocity of the impactor was 18 mph.

Figure 23 shows the impactor force versus travel with LN2 at 77 and 92 K. The LN2 at 77 K has a slightly stiffer response which can be attributed to its higher density, viscosity, and bulk modulus.

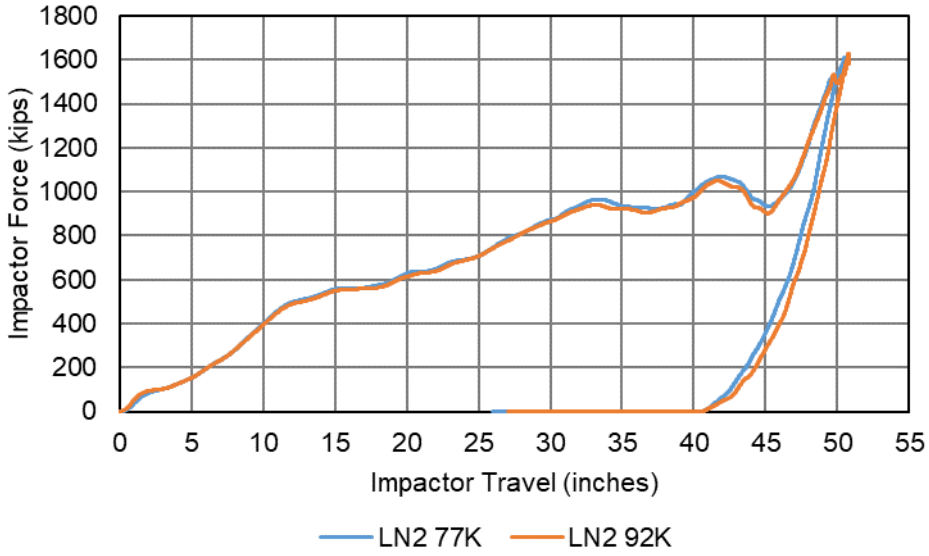

Figure 23. Impactor Force vs. Travel for Non-puncture FE Model Impacted at 18 mph with LN2 at 77 and 92 K

Figure 24 shows the outage pressure versus time with LN2 at 77 and 92 K. A larger increase in pressure was observed in the case with LN2 at 77 K even though impactor travel was lower. Typically, if the impactor travels further, there is more pressure increase because the volume of the tank car has been reduced to a greater degree. In this case the reverse was observed because the LN2 was less compressible at 77 K. With the LN2 being less compressible, more compression occurred in the gaseous N2 as the tank's volume was reduced by the impact.

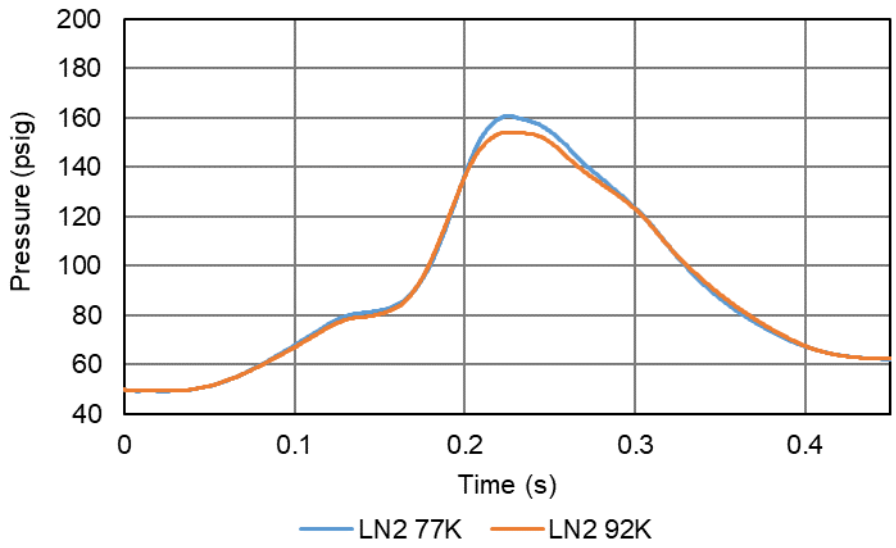

Figure 24. Outage Pressure vs. Time for Non-puncture FE Model Impacted at 18 mph with LN2 at 77 K and 92 K

Because the exact temperature of the LN2 that would be used for Test 12 was unknown when the pre-test modeling started, a temperature of 77 K was assumed as a slightly worse case scenario to cause puncture because of the stiffer response to a side impact.

5. Conclusion

This report documents the efforts of Volpe to analyze the side impact puncture performance of a surrogate DOT-113 tank car filled with cryogenic LN2 in anticipation of performing an impact test under this loading condition. Since this will be the first side impact test using LN2, a series of incremental analyses occurred to transition from a validated post-test model of a DOT-113 surrogate filled with water at room temperature to a pre-test model of a DOT-113 surrogate filled with LN2 at cryogenic temperature. The post-test model from Test 11 was incrementally simplified to represent a generalized DOT-113 surrogate with the initial conditions from Test 11. The generalized model was then incrementally modified to represent the planned test conditions for Test 12 and the overall effect of each incremental change was investigated.

This report examines the thermal contraction behavior expected in the inner vessel as the DOT-113 surrogate is cooled and loaded with LN2 prior to Test 12. The model results indicated that the through-thickness temperature would reach equilibrium in a much shorter time than it would take to fill the tank. Thus, the tank can be assumed to be at a uniform temperature at the beginning of the test. Additionally, the thermal contraction resulted in a very small (0.8%) reduction in the volume of the inner vessel, with fairly small thermally-induced stresses. On the basis of these results, the pre-test puncture model can be run using nominal (i.e., warm) dimensions for the tank and can neglect the stresses that develop from thermal contraction without expecting to significantly affect the model's results.

The effects of using different thermodynamic assumptions were examined in modeling N2 gas as (1) an isothermal ideal gas, (2) an isothermal real gas using an iterative Redlich-Kwong approach, (3) an adiabatic ideal gas, and (4) an isobaric gas undergoing condensation. At an initial pressure of 50 psig, the model results indicated that an adiabatic ideal gas gave the stiffest force-displacement response and the isobaric gas gave the softest force-displacement response. Thus, the adiabatic gas model would be expected to estimate the lowest speed to puncture and the isobaric gas would be expected to estimate the highest speed to puncture if used in puncture-capable FE models.

The effect of temperature on the mechanical response of the LN2 was also investigated. The practical range of expected temperatures for LN2 in the DOT-113 surrogate test was 77 to 92 K. The model exhibited a slightly stiffer force-displacement response when at 77 K versus 92 K, attributed to the decreased compressibility of LN2 at 77 K. Note that the stress-strain response of the inner vessel's material would be expected to vary slightly at these different temperatures, but a single stress-strain response was used in this examination to isolate the effects of the fluid response alone.

Even though the geometry and materials of construction of the DOT-113 surrogate were carefully modeled, several modeling uncertainties remained prior to Test 12, including:

1. Changes to the compressibility of the gaseous N2 due to:
    a. Real gas intermolecular interactions
    b. Phase change
    c. Non-uniform temperature distribution
    d. Convective heat transfer

2. Changes to the plasticity and fracture of the inner vessel's stainless steel due to:
    a. Cryogenic temperature
    b. Elevated strain rate
    c. Heat generation

Additional material testing at elevated rates and temperatures were planned and expected to help address some of these uncertainties. Temperature and pressure data planned to be collected during Test 12 was also anticipated to help better understand the behaviors of LN2 and N2 within the tank under impact conditions. Thus, the results of Test 12 were expected to be used to improve the post-test model of Test 12 and inform the pre-test model for the final test of a DOT-113C120W9 using LN2 (Test 13).

6. References

[1] Trevithick, S., Carolan, M., Eshraghi, S., & Wilson, N., "Side Impact Test and Analyses of a Legacy DOT-113 Tank Car," U.S. Department of Transportation, Federal Railroad Administration, Technical Report No. DOT/FRA/ORD-21/28, Washington, DC, 2021.

[2] Wilson, N., Carolan, M., Trevithick, S., & Eshraghi, S., "Side Impact Test of a DOT-113 Surrogate Tank Car with Water," U.S. Department of Transportation, Federal Railroad Administration, Technical Report No. DOT/FRA/ORD-21/35, Washington, DC, 2021.

[3] U.S. Government Publishing Office, "Title 49 Code of Federal Regulations Section 179.16, Tank-head puncture-resistance systems," Pipeline and Hazardous Materials Safety Administration, DOT, Washington, DC, 2015.

[4] U.S. Government Publishing Office, "Title 49 Code of Federal Regulations Section 179.202-12, Performance standard requirements (DOT-117P)," Pipeline and Hazardous Materials Safety Administration, DOT, Washington, DC, 2015.

[5] ASTM International, "ASTM A240/A240M: Standard Specification for Chromium and Chromium-Nickel Stainless Steel Plate, Sheet, and Strip for Pressure Vessels and for General Applications," ASTM International, 2019.

[6] Nickel Development Institute, "Materials for Cryogenic Service: Engineering Properties of Austenitic Stainless Steels," International Nickel Limited, Report No. 4368, Durham, NC, 1974.

[7] National lnstitute of Standards and Technology, "Material Properties: 304 Stainless (UNS S30400)," NIST, n.a.

[8] Onnes, H. K., "Expression of state of gases and liquids by means of series," in *KNAW Proceedings*, 1901–1902.

[9] Redlich, O., & Kwong, J. N. S., "On the Thermodynamics of Solutions. V. An Equation of State. Fugacities of Gaseous Solutions," *Chemical Reviews,* vol. 44, no. 1, p. 233–244, 1949.

[10] National Institute of Standards and Technology, "NIST Standard Reference Database Number 69," Washington, DC: U.S. Department of Commerce.

[11] Smits, A. J., A Physical Introduction to Fluid Mechanics, New York: John Wiley and Sons, 2000.

[12] Engineering ToolBox, "Universal and Individual Gas Constants," Engineering ToolBox, 2004.

[13] Kirkpatrick, S., "Detailed Puncture Analyses of Various Tank Car Designs - Final Report - Revision 1.," Applied Research Associates, Inc., Washington, DC: U.S. Department of Transportation, Federal Railroad Administration, January 2010.

[14] Urieli, I., "Specific Heat Capacities of Air," Engineering Thermodynamics, 2008.

[15] Engineering ToolBox, "Air - Molecular Weight and Composition," 2004.

[16] Kirkpatrick, S. W., Rakoczy, P., MacNeill, R. A., & Anderson, A., "Side Impact Test and Analyses of a DOT-111 Tank Car," U.S. Department of Transportation, Federal Railroad Administration, Technical Report No. DOT/FRA/ORD-15/30, Washington DC, 2015.

[17] Rakoczy, P., & Carolan, M., "Side Impact Test and Analysis of a DOT-112 Tank Car," U.S. Department of Transportation, Federal Railroad Administration, Technical Report No. DOT/FRA/ORD-16/38, Washington, DC, 2016.

[18] Rakoczy, P., Carolan, M., Gorhum, T., & Eshraghi, S., "Side Impact Test and Analyses of a DOT-117 Tank Car," U.S. Department of Transportation, Federal Railroad Administration, Technical Report No. DOT/FRA/ORD-19/13, Washington, DC, 2019.

[19] Carolan, M., & Rakoczy, P., "Side Impact Test and Analyses of a DOT-105 Tank Car," U.S. Department of Transportation, Federal Railroad Administration, Technical Report No. DOT/FRA/ORD-19/12, Washington DC, 2019.

Appendix A.
Description of Non-puncture FE Model

In preparation for a side impact test of a DOT-113 surrogate filled with LN2, a non-puncture model of the DOT-113 surrogate tank car was analyzed with a 5 percent N2 outage initially at 92 K and 50 psig under an 18 mph impact condition. The non-puncture model is shown in Figure A1. The model contained all the features of the puncture-capable model which was used to estimate the speed to cause puncture for Test 12 except that it did not have puncture-capable "solid patch" regions in the outer and inner vessels. This version of the non-puncture model is different from the models which were used to simulate thermal contraction in Sections 2.1 and 2.2 because those models did not include modeling of the fluid or gas phases.

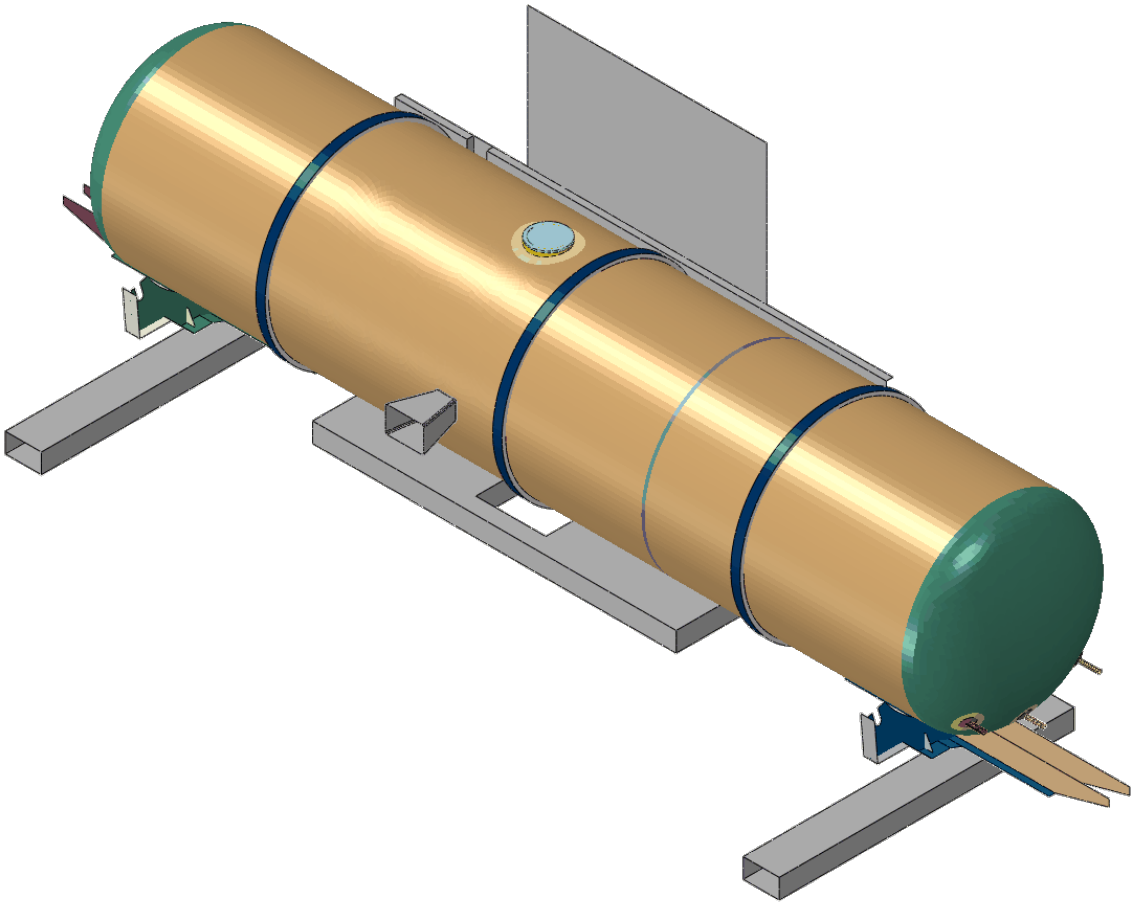

Figure A1. DOT-113 Surrogate Non-puncture FE Model

Figure A2 shows a cut view centered on the longitudinal impact plane of the DOT-113 surrogate non-puncture FE model. Within the inner vessel, the liquid lading (grey) was represented as a Lagrangian EOS and is described in Appendix A, A.4. The gas phase was represented using a pneumatic cavity with a uniform pressure and is described in Appendix A, A.3.

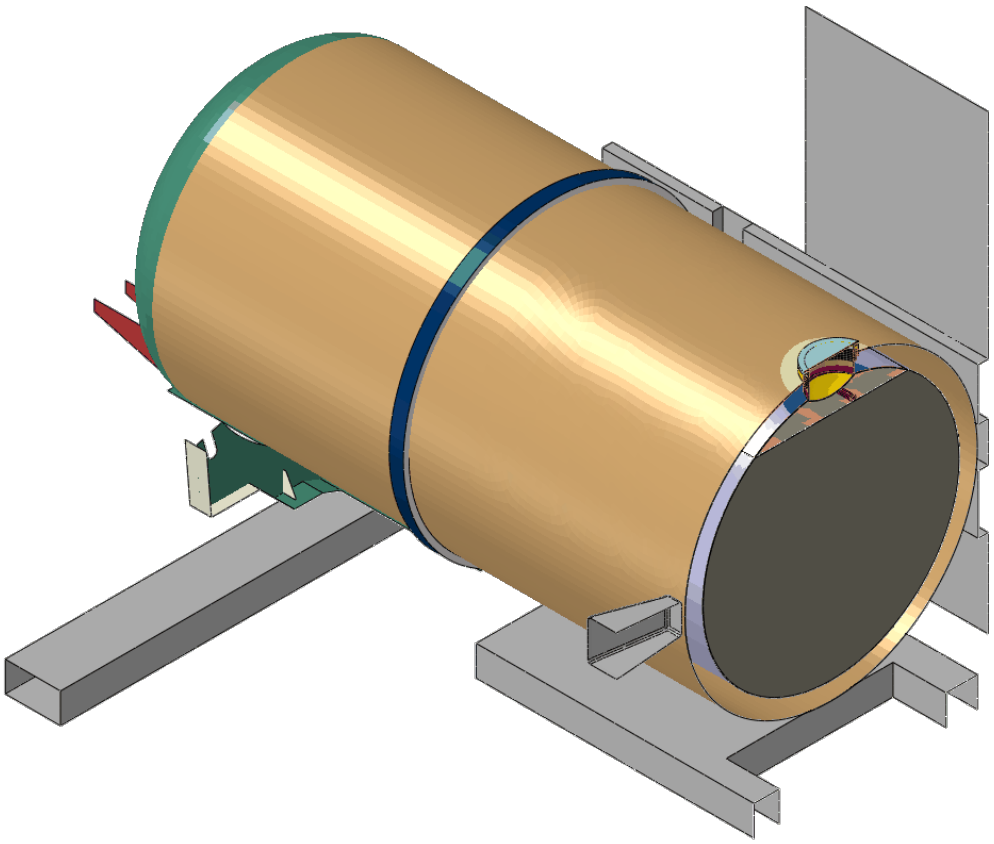

Figure A2. DOT-113 Surrogate Non-puncture FE Model Cut View

The exclusion of very small solid elements allowed for the model to run to completion approximately eight times faster. This allowed for a variety of liquid and gas modeling techniques to be applied to separately investigate the effects of: (1) adiabatic heating, (2) phase change, (3) real gas compressibility, and (4) temperature stratification. For adiabatic heating, a similar non-puncture version of the Test 11 DOT-113 surrogate was also used.

A.1. AAR TC128, Grade B Carbon Steel

Table A1 summarizes the material properties of TC128 steel used in the outer vessel of the FE model. Tensile tests on TC128 specimens cut from the outer vessel of the Test 12 DOT-113 surrogate were not conducted at the time of the pre-test modeling so the tensile test results from the Test 11 DOT-113 surrogate [2] were used. Damage progression and evolution was not specified because the model was not intended to evaluate puncture.

Table A1. Summary of Properties for TC128 Carbon Steel

Parameter	Value
Mass Density	7.35E-04 lbf-s^2/in^4

Parameter	Value
Modulus of Elasticity	3.00E+07 psi
Poisson's Ratio	0.30
Plasticity	Piecewise linear (see Figure A3 and Table A2)
Damage Initiation	N/A
Temperature	Room temperature
Strain Rate	Quasi-static
Mesh Implementation	3-inch Reduced Integration Shell (S4R, S3) Elements

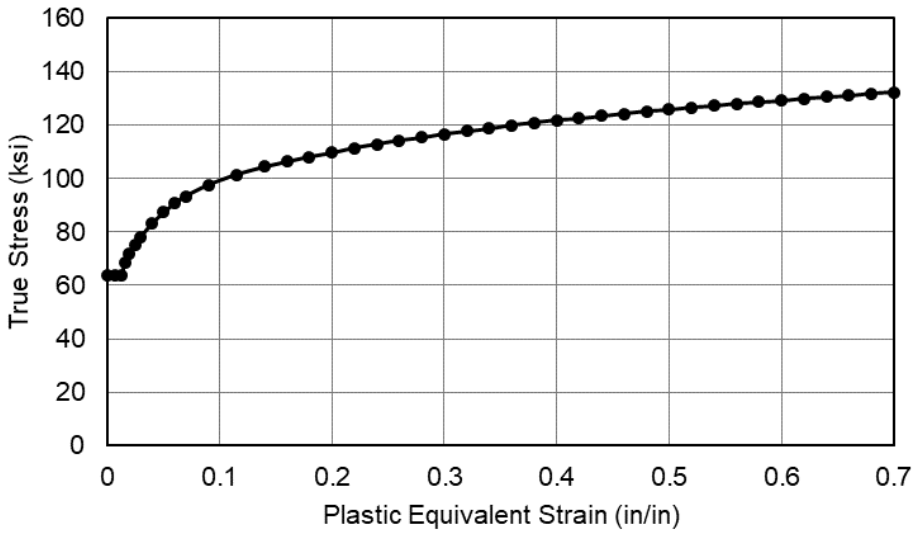

Figure A3. True Stress vs. Plastic Equivalent Strain for TC128 at Room Temperature and Quasi-static Rate

Table A2. Plastic Equivalent Strain vs. True Stress Input for TC128 Carbon Steel in DOT-113 Surrogate Outer Tank

PEEQ	True Stress	PEEQ	True Stress	PEEQ	True Stress
in/in	*ksi*	*in/in*	*ksi*	*in/in*	*ksi*
0.000E+00	6.396E+01	2.600E-01	1.142E+02	6.400E-01	1.306E+02
6.500E-03	6.396E+01	2.800E-01	1.154E+02	6.600E-01	1.312E+02
1.300E-02	6.396E+01	3.000E-01	1.166E+02	6.800E-01	1.317E+02
1.600E-02	6.838E+01	3.200E-01	1.178E+02	7.000E-01	1.323E+02

PEEQ	True Stress	PEEQ	True Stress	PEEQ	True Stress
2.000E-02	7.176E+01	3.400E-01	1.188E+02	7.200E-01	1.329E+02
2.500E-02	7.514E+01	3.600E-01	1.198E+02	7.400E-01	1.334E+02
3.000E-02	7.826E+01	3.800E-01	1.208E+02	7.600E-01	1.339E+02
4.000E-02	8.346E+01	4.000E-01	1.217E+02	7.800E-01	1.345E+02
5.000E-02	8.736E+01	4.200E-01	1.226E+02	8.000E-01	1.350E+02
6.000E-02	9.074E+01	4.400E-01	1.235E+02	8.200E-01	1.355E+02
7.000E-02	9.334E+01	4.600E-01	1.243E+02	8.400E-01	1.359E+02
9.000E-02	9.750E+01	4.800E-01	1.251E+02	8.600E-01	1.364E+02
1.150E-01	1.014E+02	5.000E-01	1.258E+02	8.800E-01	1.369E+02
1.400E-01	1.045E+02	5.200E-01	1.266E+02	9.000E-01	1.373E+02
1.600E-01	1.063E+02	5.400E-01	1.273E+02	9.200E-01	1.378E+02
1.800E-01	1.081E+02	5.600E-01	1.280E+02	9.400E-01	1.382E+02
2.000E-01	1.098E+02	5.800E-01	1.287E+02	9.600E-01	1.387E+02
2.200E-01	1.114E+02	6.000E-01	1.293E+02	9.800E-01	1.391E+02
2.400E-01	1.128E+02	6.200E-01	1.299E+02	1.000E+00	1.395E+02

Figure A4 shows the nominal stress-strain response from a FE model of a 2-inch gage length (GL) smooth round bar (SRB) specimen. The TC128 SRB FE model is described in the Test 11 report [2]. The specimen used a 0.083-inch C3D8R mesh.

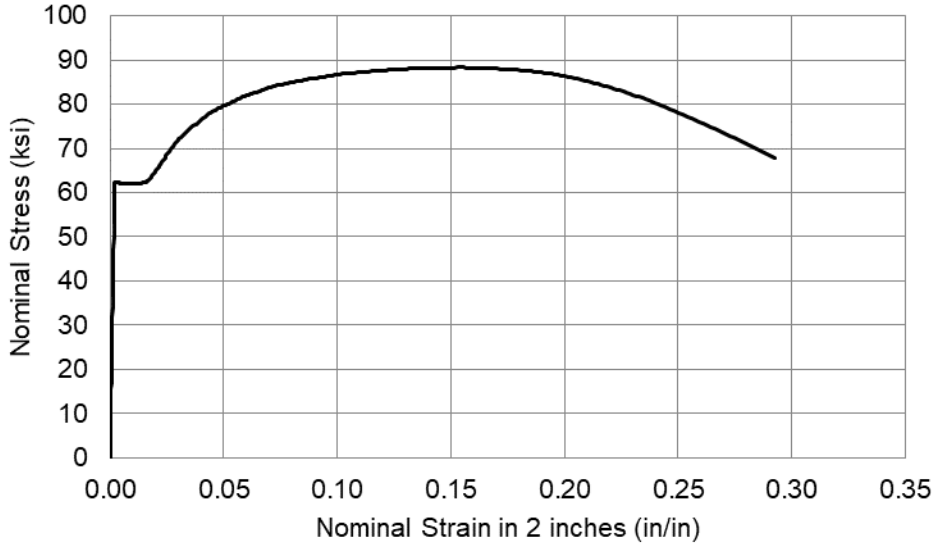

Figure A4. Nominal Stress vs. Strain in 2-inches for TC128 at Room Temperature and Quasi-static Rate

A.2. ASTM A240 Type 304 Stainless Steel

Table A3 summarizes the material properties used for the T304 steel inner vessel in the FE model of the DOT-113 surrogate tank car. Damage progression and evolution was not specified because the model was not intended to evaluate puncture. This table includes the unit system used in the FE model.

Table A3. Summary of Properties for T304 Stainless Steel

Parameter	Value
Mass Density	7.35E-04 lbf-s^2/in^4
Modulus of Elasticity	3.00E+07 psi
Poisson's Ratio	0.29
Plasticity	Piecewise linear (see Figure A5)
Damage Initiation	N/A
Temperature	111 K
Strain Rate	1 in/in/s
Mesh Implementation	3-inch Reduced Integration Shell (S4R, S3) Elements

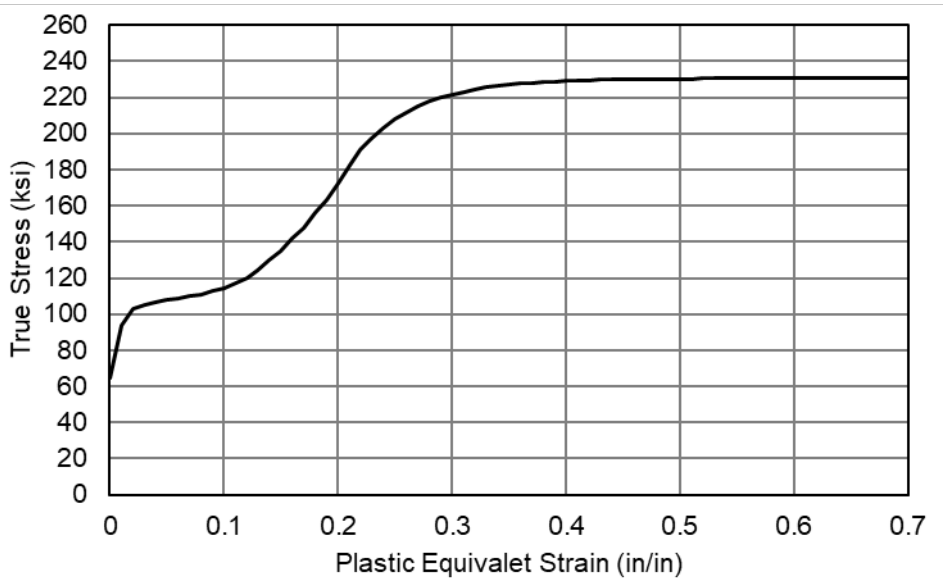

Figure A5. True Stress vs. Plastic Equivalent Strain for Stainless Steel T304 at 111 K and 1 in/in/s

Figure A6 shows the nominal stress-strain response from a FE model of a 2-inch GL SRB specimen. The SRB FE model is described in the Test 11 report [2]. The specimen used a 0.05-inch C3D8R mesh.

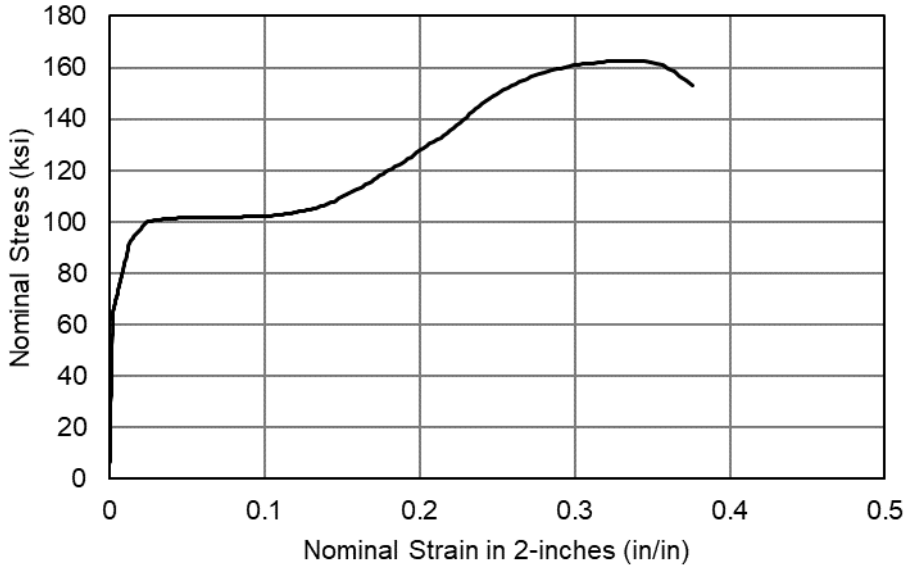

Figure A1. Nominal Stress vs. Strain in 2-inches for Stainless Steel T304 at 111 K and 1 in/in/s

A.3. Gaseous Nitrogen

The gas phase of the lading was modeled as N2 at a gauge pressure of 50 psi (62.3 psia), as this was the desired internal pressure for the tank car at the beginning of the test. Within Abaqus, the N2 within the outage was modeled as an ideal gas, using a pneumatic cavity modeling technique. This modeling technique requires a surface to be defined that encloses the cavity, with a reference point defined within this cavity to which initial temperature and pressure can be assigned.

The pneumatic cavity approach models the entire cavity with a single uniform pressure and uniform temperature value. The air pressure within the model was allowed to change as the volume of the tank changed due to the impact while the temperature was held constant. Table A4 summarizes the modeling inputs defined for the air phase of the model. This table includes the unit system used in the FE model.

Table A1. Properties for Nitrogen (Pneumatic Cavity)

Property	Value	Reference
Universal Gas Constant (R)	73.583 in-lbf/(mol-K)	[12]
Molecular Weight (MW)	1.5996E-4 lbf-s^2/(mol-in)	[10]
Constant Temperature	92 K	
Molar Specific Heat ($c_{p,m}$)	257.59 in-lbf/(mol-K)	[10]
Initial Pressure	50 psig	

The molar specific heat capacity at constant pressure ($c_{p,m}$) for air was calculated according to Equation A1.

Equation A1. Calculation of Molar Specific Heat

$$C_{P \cdot m} = C_P \cdot MW$$

A.4. LN2

The target initial conditions for the side impact test of the surrogate DOT-113 tank car were set to an outage volume of 5 percent and internal pressure of 50 psig. The liquid phase of the lading was modeled as LN2 at temperatures of 77 and 92 K. Within Abaqus, a Lagrangian EOS model describes the behavior of LN2. The fluid was meshed with 3-inch fully integrated brick (C3D8) elements. The key material properties that must be input to this material model are the material's density, dynamic viscosity, and bulk modulus. These values were obtained from the NIST standard at a constant pressure of 62.3 psia [10].

Table A5 summarizes the properties of the LN2 included in the DOT-113 surrogate FE model. The temperature dependent material properties are shown in Table A6. These tables include the unit system used in the FE model.

Table A5. Summary of Properties for LN2

Parameter	Value
Mass Density	Temperature dependent (see Table A6)
Initial Pressure	62.3 psia
Initial Temperature	77 K or 92 K
Sound Speed	Temperature dependent (see Table A6)
Bulk Modulus	Temperature dependent (see Table A6)
Mesh Implementation	3-inch Fully Integrated Brick (C3D8) Elements

Table A6. Fluid Properties of LN2 at 62.3 psia vs. Temperature

Temperature	Viscosity	Density	Sound Speed	Bulk Modulus
Kelvin	*psi-s*	*lbf-s^2/in^4*	*in/s*	*psi*
64	4.3021E-08	8.0890E-05	3.8941E+04	1.2266E+05
65	4.0863E-08	8.0504E-05	3.8541E+04	1.1958E+05
66	3.8854E-08	8.0116E-05	3.8142E+04	1.1655E+05
67	3.6983E-08	7.9726E-05	3.7745E+04	1.1358E+05
68	3.5237E-08	7.9333E-05	3.7348E+04	1.1066E+05
69	3.3605E-08	7.8937E-05	3.6952E+04	1.0778E+05
70	3.2081E-08	7.8537E-05	3.6556E+04	1.0495E+05
71	3.0655E-08	7.8136E-05	3.6160E+04	1.0217E+05
72	2.9319E-08	7.7732E-05	3.5764E+04	9.9423E+04
73	2.8066E-08	7.7324E-05	3.5367E+04	9.6720E+04
74	2.6890E-08	7.6912E-05	3.4970E+04	9.4058E+04
75	2.5785E-08	7.6497E-05	3.4572E+04	9.1434E+04
76	2.4745E-08	7.6079E-05	3.4174E+04	8.8848E+04
77	2.3766E-08	7.5657E-05	3.3773E+04	8.6297E+04
78	2.2842E-08	7.5231E-05	3.3371E+04	8.3781E+04
79	2.1970E-08	7.4802E-05	3.2968E+04	8.1300E+04
80	2.1148E-08	7.4368E-05	3.2562E+04	7.8852E+04
81	2.0368E-08	7.3930E-05	3.2154E+04	7.6436E+04
82	1.9631E-08	7.3486E-05	3.1744E+04	7.4051E+04
83	1.8930E-08	7.3038E-05	3.1331E+04	7.1697E+04
84	1.8266E-08	7.2585E-05	3.0915E+04	6.9374E+04
85	1.7635E-08	7.2127E-05	3.0496E+04	6.7080E+04
86	1.7035E-08	7.1662E-05	3.0074E+04	6.4812E+04
87	1.6462E-08	7.1192E-05	2.9648E+04	6.2576E+04
88	1.5915E-08	7.0715E-05	2.9217E+04	6.0364E+04
89	1.5393E-08	7.0231E-05	2.8782E+04	5.8179E+04
90	1.4892E-08	6.9740E-05	2.8342E+04	5.6020E+04
91	1.4414E-08	6.9241E-05	2.7897E+04	5.3887E+04
92	1.3955E-08	6.8735E-05	2.7446E+04	5.1778E+04

A.5. Membrane

An artificial surface was modeled within the tank to define the limits of the pneumatic cavity (outage). Frictionless, hard contact was assigned between the membrane and the inner vessel and

lading. Because this surface does not correspond to any physical feature within the tank, modeling techniques were chosen to minimize the increase in either mass or stiffness introduced into the model by the membrane while not negatively impacting the FE model's stability or runtime. The material properties of the membrane are summarized in Table A7. This table includes the U.S. customary units used in the FE model.

Table A7. Material Properties Defined for Membrane Material

Parameter	**Value**
Density	7.35E-06 lbf-s^2/in^4
Modulus of Elasticity	1.00E+04 psi

Appendix B.
Thermal Contraction of Inner Vessel Through Thickness

Figure B1 shows the FE model of the surrogate inner vessel and the three DOF translation constraint on the nodes in the longitudinal center.

Figure B2 shows the temperature distribution of the tank car after 30 seconds from analysis. It can be seen that the entire tank car has reached the steady state condition in that time period.

Figures B3 through B5 show the magnitude, radial and longitudinal deformations of the inner vessel respectively. Since the deformations are plotted with respect to a Cartesian co-ordinate system, the radial deformation plot shows the deformation with respect to one radial co-ordinate axis.

Figure B6 shows the von-Mises stress plot of the inner vessel. For stability reasons, a circumferential constraint was used on the outer surface nodes of the tank exactly at the longitudinal center of the tank. Since that constraint unrealistically resisted radial contraction in that zone, a high stress value is seen in this plot and can be ignored. The actual inner vessel support system was not included for this model because details were not finalized at the time of this modeling effort. The thermal contraction results presented in Section 2.2 used a detailed model that featured a more accurate representation of the actual support system and had stress levels in that region that were an order of magnitude lower.

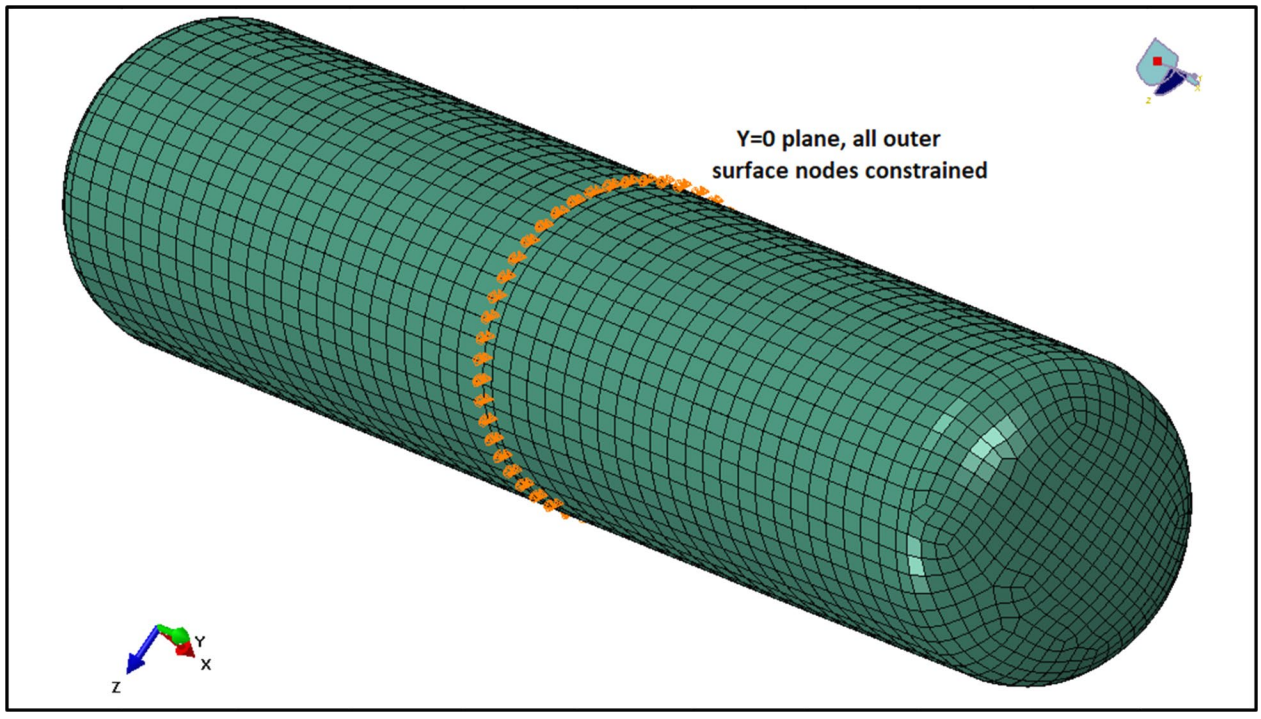

Figure B1. FE Model of the Surrogate Inner Vessel

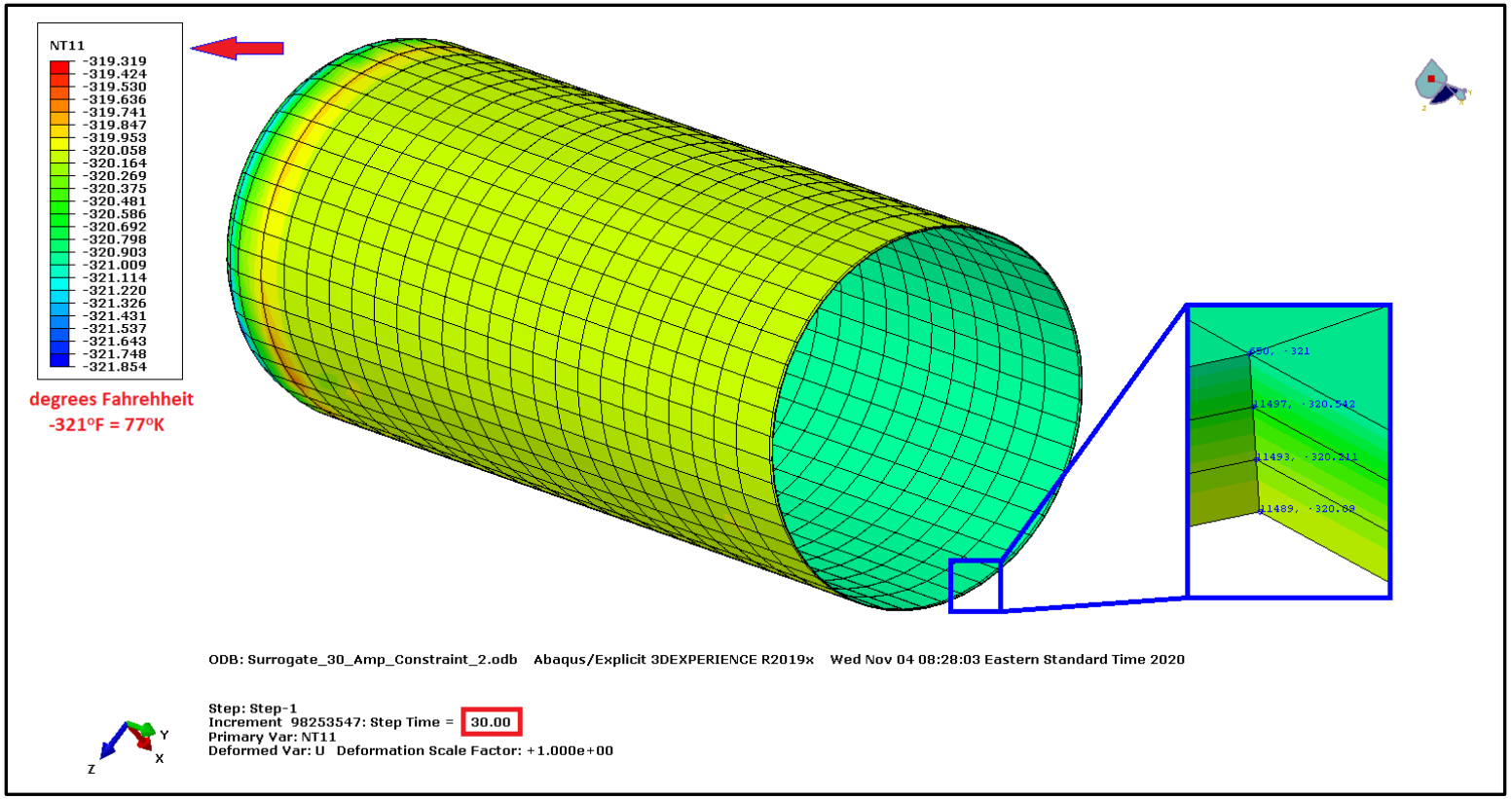

Figure B2. Steady State Temperature Contour Plot at 30 Seconds – Cross Sectional View of Tank

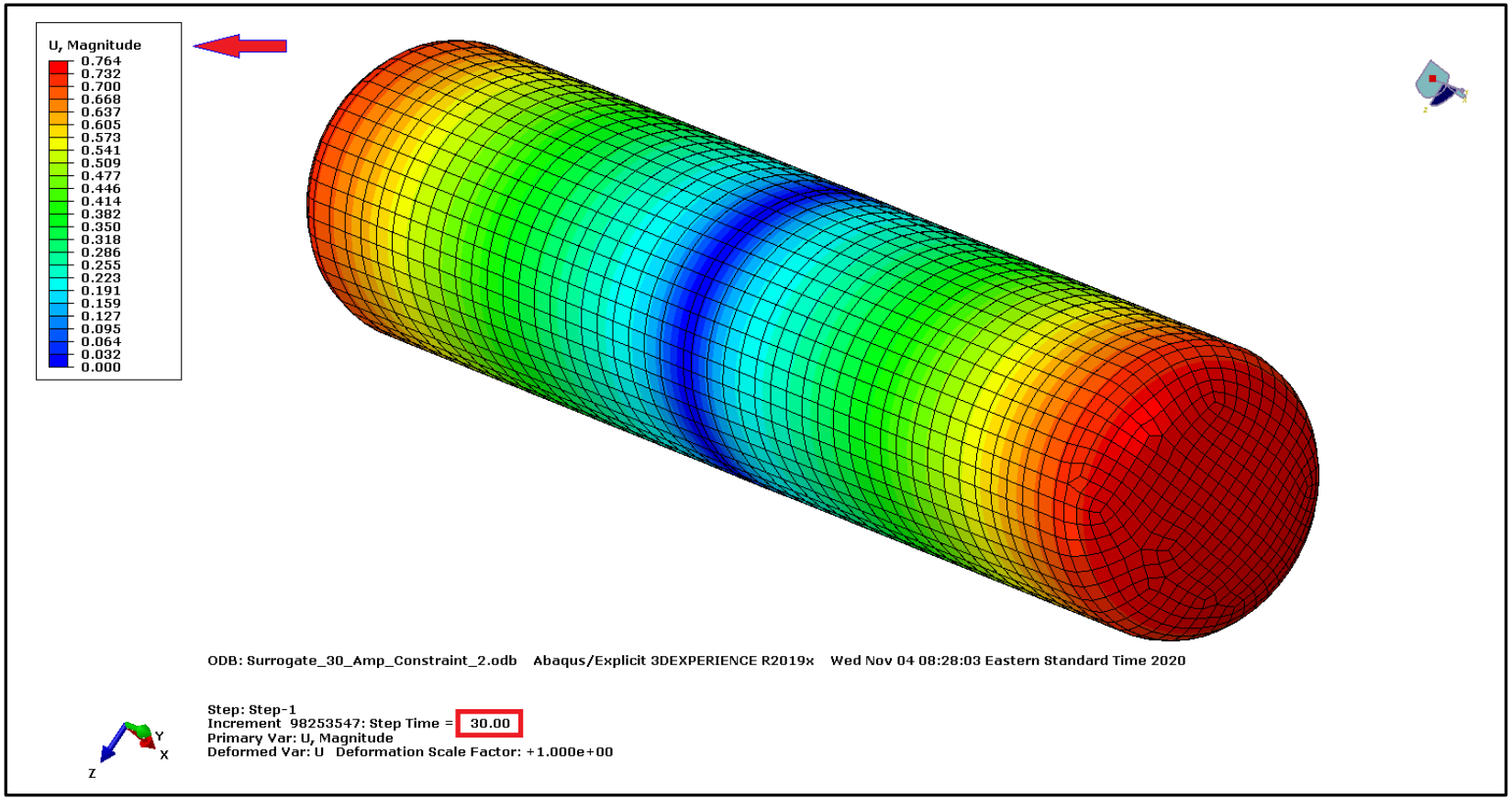

Figure B3. Displacement Magnitude Plot of the Tank at 30 Seconds

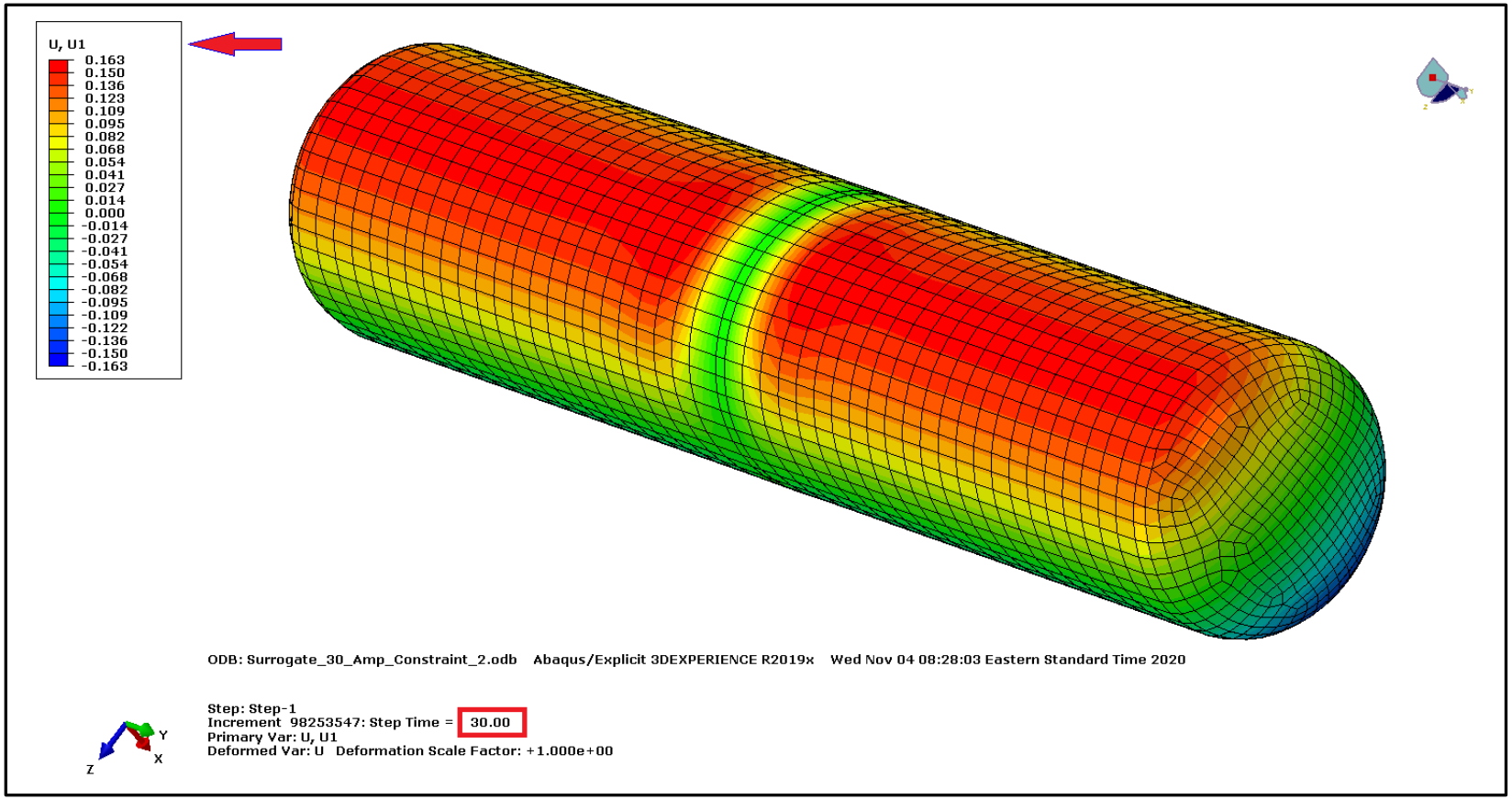

Figure B4. Displacement Plot in the Radial Direction at 30 Seconds

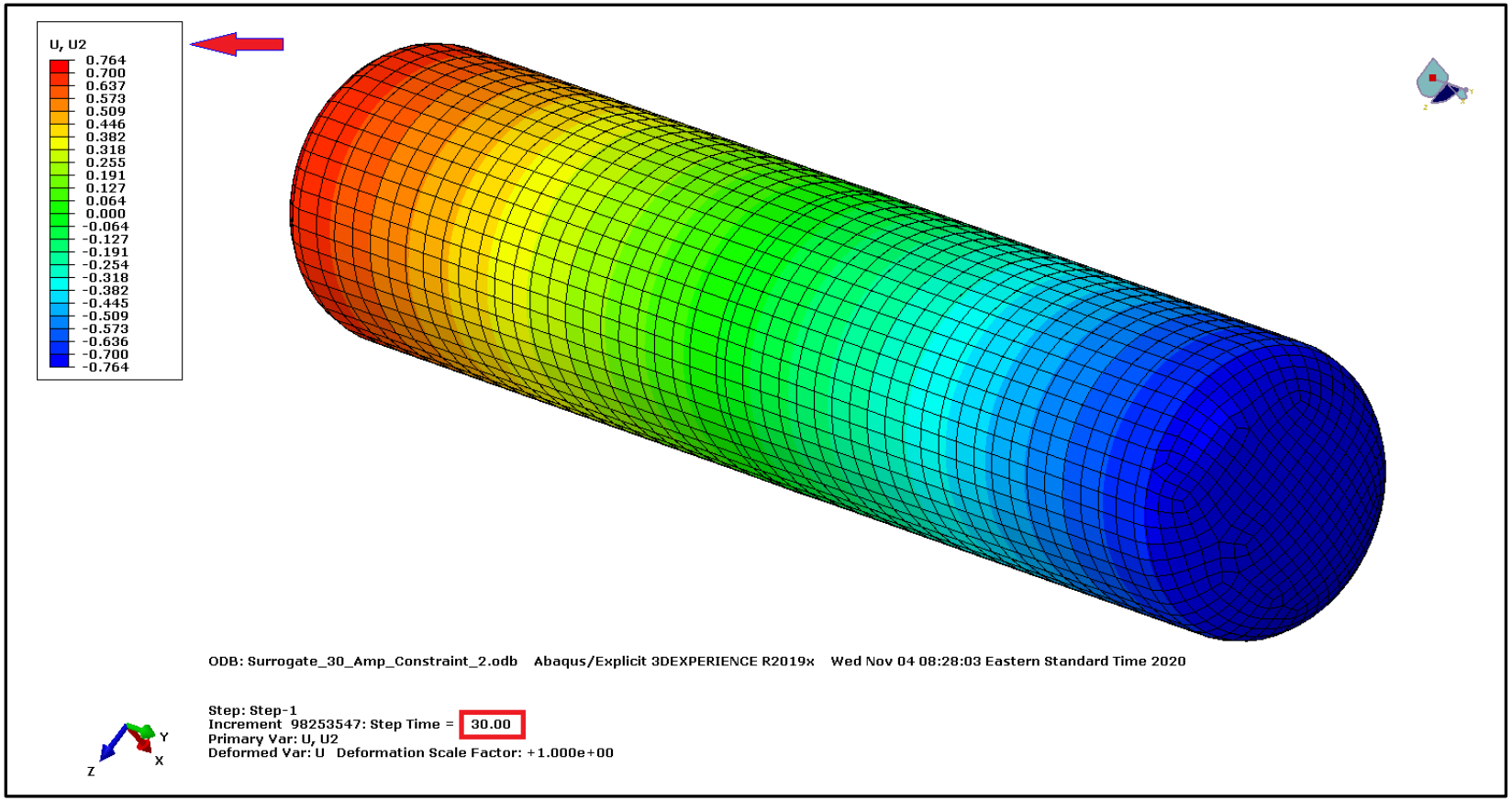

Figure B5. Displacement Plot in the Longitudinal Direction at 30 Seconds

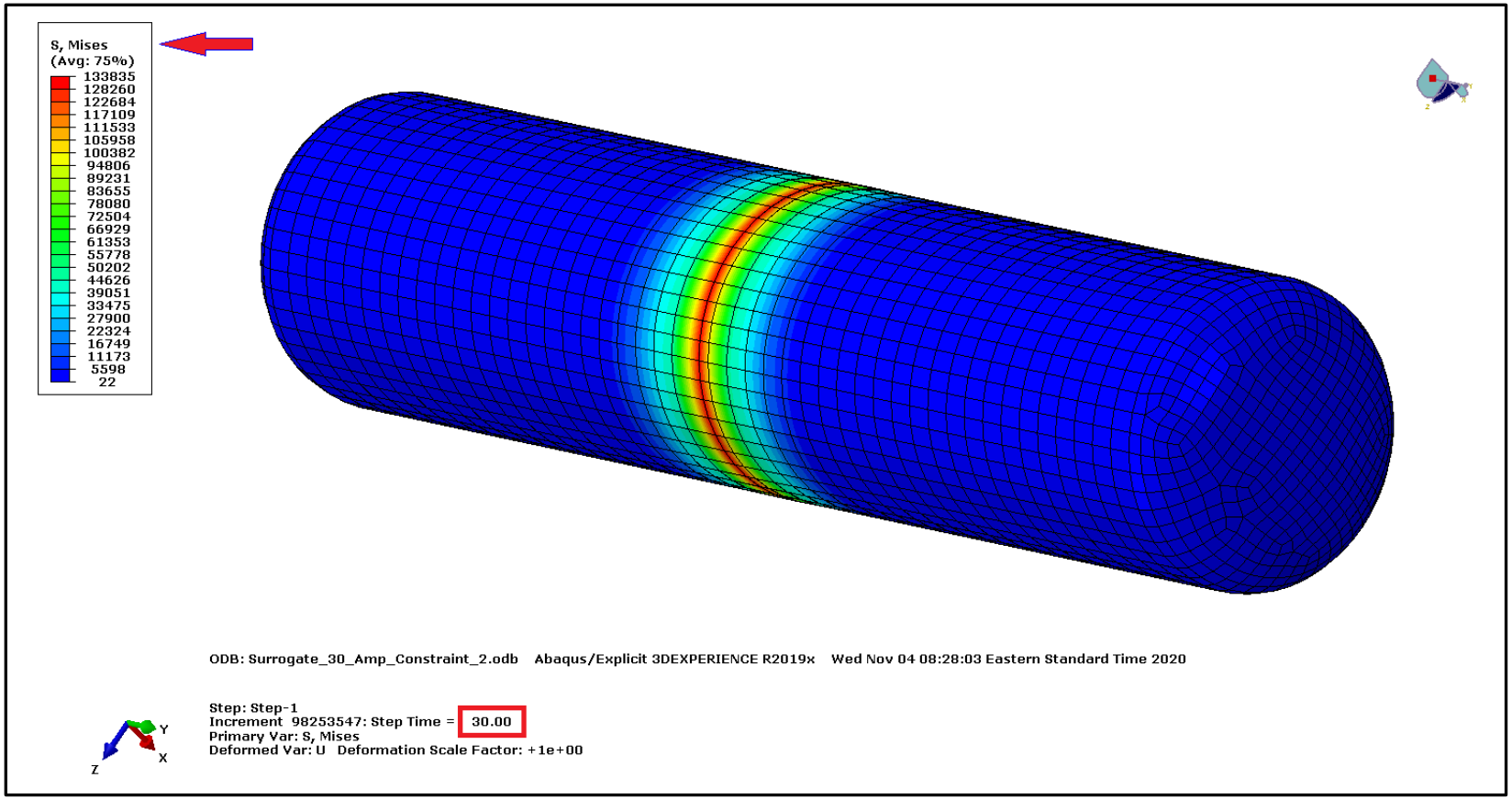

Figure B6. von Mises Stress Plot of the Tank at 30 Seconds

Abbreviations and Acronyms

ACRONYMS	EXPLANATION
T304	ASTM A240 Type 304 Stainless Steel
ASTM	American Society for Testing and Materials
AAR	Association of American Railroads
TC128	AAR TC128, Grade B Carbon Steel
DOF	Degrees of Freedom
DOT	Department of Transportation
d	Diameter
EOS	Equations of State
FRA	Federal Railroad Administration
FEA	Finite Element Analysis
GL	Gage Length
HMR	Hazardous Materials Regulations
kip	Kilopound (1,000 lbf)
LNG	Liquefied Natural Gas
LN2	Liquid Nitrogen
MLI	Multi-layer Insulation
NIST	National Institute of Standards and Technology
N2	Nitrogen
NPRM	Notice of Proposed Rulemaking
PHMSA	Pipeline and Hazardous Materials Safety Administration
PEEQ	Plastic Equivalent Strain
PRV	Pressure Relief Valve
SPH	Smoothed Particle Hydrodynamic
SRB	Smooth Round Bar
STDP	Start to Discharge Pressure
t	Thickness
TTC	Transportation Technology Center (the site)
TTCI	Transportation Technology Center, Inc. (the company)
Volpe	Volpe National Transportation Systems Center